Research Square

Preprints are preliminary reports that have not undergone peer review.
They should not be considered conclusive, used to inform clinical practice,
or referenced by the media as validated information.

Distributed Event-Triggered Adaptive Coordination of Uncertain Multi-Agent Systems with Neural-Network Compensation

hongjie Li

hongjie_lee@zjxu.edu.cn

Jiaxing University

Jinde Cao

Southeast University

Research Article

Keywords:

Posted Date: November 24th, 2026

DOI: https://doi.org/10.21203/rs.3.rs-11662418/v1

License: This work is licensed under a Creative Commons Attribution 4.0 International License.
Read Full License

Additional Declarations: No competing interests reported.

Distributed Event-Triggered Adaptive Coordination of Uncertain Multi-Agent Systems with Neural-Network Compensation

Hongjie Li[1] and Jinde Cao[2]

[1]College of Data Science, Jiaxing University, Jiaxing, 314001, Zhejiang, China.
[2]School of Mathematics, Southeast University, Nanjing, 211189, China.

Contributing authors: hongjie_lee@zjxu.edu.cn; jdcao@seu.edu.cn;

Abstract

This study addresses consensus and tracking for uncertain second-order multi-agent systems with nonlinear restoring and damping effects and bounded external disturbances. An adaptive event-triggered controller with separated information channels is proposed. Sampled-and-held aggregate measurements enter the linear coupling term; the robust feedback and neural-network adaptation laws, in contrast, use the current local aggregate. This structure retains the cancellations needed in the Lyapunov analysis while restricting event-triggered updates to the coupling channel. Under a stabilizability-based linear matrix inequality, suitable graph-dependent gain conditions, bounded neural approximation errors, and a compact approximation-domain condition, complete leaderless consensus and asymptotic leader–follower tracking are established. The analysis also provides exponential error bounds and rules out finite-time accumulation of triggering instants. Two ten-agent examples illustrate the design: constrained-guideway vehicle coordination with nonlinear rolling resistance, and coupled nonlinear oscillators tracking a disturbed leader through sparse pinning. Their numerical results cover state responses, control effort, update patterns, disturbance and threshold sensitivity, and integration-grid refinement. Finite-record excitation diagnostics are reported separately; state coordination alone is not taken as evidence of neural-weight convergence.

Keywords: Nonlinear multi-agent systems; dynamic event-triggered control; adaptive neural control; robust consensus; leader–follower tracking

1 Introduction

Multi-agent models arise in mechanical coordination, vehicle motion, and oscillator networks. In these applications, the interaction among agents is only part of the control problem. Each unit may also exhibit nonlinear restoring forces, velocity-dependent resistance, and uncertain external loads. Such effects can influence transient behavior and the effort required to achieve coordination. A useful controller must therefore address the nonlinear agent dynamics and the communication demands of the network at the same time.

Adaptive neural control provides one way to compensate for uncertain nonlinear terms. Its use in multi-agent synchronization and consensus has been studied for higher-order systems, time-delay models, heterogeneous agents, and leader–follower configurations [1–8]. Related results address robust containment, prescribed-performance objectives, and switching or communication-constrained networks [9, 11–13]. Neural approximation has also

been incorporated into distributed formation control for uncertain underactuated surface vehicles, including designs with asynchronous edge-based communication and disturbance compensation [37]. These studies establish the usefulness of adaptive approximation in networked nonlinear control. A separate issue, however, concerns the behavior of the estimated weights. Convergence of the coordination error does not, by itself, imply convergence of the neural parameters. As the agents approach a coordination manifold, the state trajectories may provide progressively less information for identifying the ideal weights.

Event-triggered methods offer a way to reduce communication updates by transmitting information only when a prescribed condition is met. Their application to multi-agent control includes nonlinear and Euler–Lagrange systems, input-constrained dynamics, formation control, and networks subject to faults or cyber-attacks [14–16, 18–23, 25, 26]. Dynamic event-triggered neural resilient control has further been considered for switched multi-agent systems exposed to attacks [17]. In parallel, adaptive double-event mechanisms have been developed for high-order fully actuated nonlinear agents [24]; neural adaptive event-triggered designs have been studied for second-order systems with time delays [36]; and asynchronous edge-triggered schemes have been proposed for sampled communication [39]. A dual-channel adaptive event-triggered strategy for predefined-time consensus provides another example of assigning distinct triggering rules to different information paths [31]. In that design, an adaptive trigger is placed in the sensor-to-controller channel and is combined with a predefined-time extended-state observer. Double-event designs, in turn, distinguish compensation updates from communication updates. The present controller uses a different split: it has one aggregate-buffer triggering rule, but only the linear coupling uses the held aggregate; the robust and adaptive channels retain current local measurements. This distinction is central to the Lyapunov estimate and should not be confused with a two-trigger communication architecture.

Other strands of research focus on observer-based coordination and communication under adverse network conditions. Adaptive memory triggering with observer-based compensation, for example, has been applied to high-speed train consensus tracking under denial-of-service attacks [10]. Further studies consider neural-network-based integral reinforcement learning, quantized active-suspension control, prescribed-time tracking, formation-containment under DoS attacks, and sampling-based reachable-set synthesis [27–30, 32, 33]. These approaches target different combinations of communication constraints, input limitations, attack resilience, and reduced monitoring. Broader perspectives on event-triggered consensus and communication in multi-agent systems can be found in [34, 35].

Among the cited studies, the neural adaptive consensus design of Yue et al. [13] is particularly close in its use of linear and discontinuous feedback for leaderless consensus and leader–follower tracking. More recent work has combined neural approximation with dynamic event triggering for delayed second-order agents [36], switched systems under attacks [17], high-order systems with double-event mechanisms [24], and predefined-time consensus through dual-channel triggering [31]. Asynchronous edge-based communication has also been studied for uncertain surface-vehicle formation control [37]. These results make clear that neither neural compensation nor dynamic event triggering alone is the principal distinction of the present study.

The point addressed here is the placement of the sampled signal within the controller. Only the linear coupling term uses a sampled-and-held aggregate. The robust sign feedback and the adaptive update directions retain the current local aggregate. This allocation preserves the direct cancellation between the nonsmooth feedback and the matched disturbance/approximation residual, while the sampling mismatch is confined to the linear coupling term and is absorbed by the dynamic trigger. Proposition 1 quantifies the additional residual that would arise if the robust sign term were also evaluated from a held aggregate. The guarantees remain conditional on graph-dependent sufficient inequalities and confinement of the plant states to the approximation domain. In addition, the current aggregate must be available through a local sensing or measurement channel, and the gain condition requires graph-level spectral information. The proposed method therefore does not establish topology-independent performance, fully distributed gain selection, or packet-level communication savings.

The nonlinear dynamics are retained explicitly in the numerical models. In particular, the examples include bounded state-dependent restoring and damping terms in the acceleration equations; the simulated responses are therefore not generated by a nominal linear plant alone. The purpose is to study coordination under uncertain mechanical-type nonlinearities and external excitation. On the theoretical side, the analysis treats matched uncertainties and bounded disturbances. It also requires stabilizability of the plant pair and closed-loop trajectories that remain inside the region where the neural approximation bounds hold. Neural weights are used as compensation variables. Persistent excitation is not required for the consensus or tracking results, and convergence to ideal neural parameters is not asserted. Finite-horizon excitation measures are instead included as separate diagnostics to clarify the difference between state regulation and parameter identification.

The communication metrics also need to be interpreted in light of the information structure. An event refreshes an agent's aggregate buffer. The reported counts therefore measure updates of the held coupling signals, not the number of individual packets exchanged among neighboring agents. Current aggregate information is assumed to be available through the local sensing channel used by the robust feedback and adaptation laws. Consequently, the event counts do not represent the full sensing, computation, or network-transmission burden.

The contributions are threefold. First, a split-information adaptive controller is formulated for leaderless consensus and leader–follower tracking. Only the linear coupling channel uses a sampled-and-held aggregate; the robust sign feedback and adaptive update directions use current local aggregate information. This choice preserves the cancellation structure of the adaptive Lyapunov argument and confines event-triggered refreshing to the coupling channel. Second, sufficient coordination conditions are derived by combining a plant-side linear matrix inequality (LMI), graph spectral quantities, and explicit bounds on neural approximation errors and disturbances. Under the stated assumptions, the results give exponential bounds for disagreement and tracking errors, complete consensus in the leaderless setting, asymptotic tracking in the leader–follower setting, and exclusion of finite-time event accumulation. The leaderless analysis also establishes convergence of the robust gains to prescribed agent-dependent targets and, under a common adaptation-rate condition, uniform boundedness of the unweighted adaptive states. Third, two ten-agent examples are used to assess finite-horizon coordination, aggregate-buffer updates, and sensitivity to disturbance magnitude, initial threshold values, and numerical-grid resolution. Both a 1-ms periodic scheme and a terminal-error-matched periodic benchmark are included. The comparison indicates that the update reduction depends on the coordination task. Separate excitation and least-squares calculations provide finite-record information about neural-weight estimation without treating parameter identification as a prerequisite for state coordination.

The remainder of the paper is organized as follows. Section 2 specifies the uncertain agent model, communication graph, coordination errors, and assumptions. Section 3 develops the adaptive event-triggered controller and establishes its properties for leaderless consensus and leader–follower tracking. Numerical evaluations, including periodic benchmarks and sensitivity tests, are presented in Section 4. Section 5 concludes the paper and discusses possible extensions.

Notation. The symbols $\|\cdot\|$ and $\|\cdot\|_F$ denote the Euclidean and Frobenius norms, respectively. For a vector x, $\|x\|_1$ and $\|x\|_\infty$ denote its ℓ_1- and ℓ_∞-norms. The operator $\mathrm{col}(\cdot)$ stacks its arguments into a column vector. For a symmetric matrix M, $\lambda_{\min}(M)$ and $\lambda_{\max}(M)$ are its smallest and largest eigenvalues. At the origin, the discontinuous map $\mathrm{sgn}(\cdot)$ is interpreted in the Filippov sense.

2 Problem Formulation and Preliminaries

Consider N agents with matched nonlinearities and bounded exogenous inputs governed by

$$\dot{x}_i(t) = Ax_i(t) + B[u_i(t) + f_i(x_i(t)) + d_i(t)] \quad (2.1)$$

for $i = 1, 2, \ldots, N$, where $x_i(t) \in \mathbb{R}^n$ and $u_i(t) \in \mathbb{R}^m$ are the state and input of agent i, with $m \leq n$. The unknown continuous map $f_i(\cdot) : \mathbb{R}^n \to \mathbb{R}^m$ and the measurable disturbance $d_i(t) \in \mathbb{R}^m$ act through the same input matrix B, and $\|d_i(t)\|_\infty \leq d_{iM}$ almost everywhere. The pair (A, B) is assumed stabilizable.

Remark 1 Model (2.1) covers several commonly used agent models ($i = 1, 2, \ldots, N$).

Case 1: If $m = n$, $A = 0_{n\times n}$, and $B = I_n$, then (2.1) reduces to the first-order nonlinear MAS

$$\dot{x}_i(t) = f_i(x_i(t)) + u_i(t) + d_i(t)$$

Case 2: If $A = \begin{bmatrix} 0 & 1 \\ 0 & 0 \end{bmatrix}$ and $B = \begin{bmatrix} 0 \\ 1 \end{bmatrix}$, then (2.1) reduces to the second-order nonlinear MAS

$$\begin{cases} \dot{x}_{i1} = x_{i2}, \\ \dot{x}_{i2} = f_i(x_i) + u_i + d_i, \end{cases}$$

Case 3: If

$$A = \begin{bmatrix} 0 & 1 & 0 & \cdots & 0 \\ 0 & 0 & 1 & \cdots & 0 \\ \vdots & \vdots & \vdots & \ddots & \vdots \\ 0 & 0 & 0 & \cdots & 1 \\ 0 & 0 & 0 & \cdots & 0 \end{bmatrix} \qquad B = \begin{bmatrix} 0 \\ 0 \\ \vdots \\ 0 \\ 1 \end{bmatrix}.$$

then (2.1) reduces to the higher-order nonlinear MAS

$$\begin{cases} \dot{x}_{i1} = x_{i2}, \\ \dot{x}_{i2} = x_{i3}, \\ \quad \vdots \\ \dot{x}_{i,n-1} = x_{in}, \\ \dot{x}_{in} = f_i(x_i) + u_i + d_i, \end{cases}$$

Case 4: If $f_i(x_i(t)) = 0_{m\times 1}$ and $d_i(t) = 0_{m\times 1}$, then (2.1) reduces to the linear MAS

$$\dot{x}_i(t) = Ax_i(t) + Bu_i(t)$$

Lemma 1 *If the pair (A, B) is stabilizable, then there exist a symmetric positive-definite matrix P and a scalar $\varrho > 0$ such that*

$$AP + PA^T - \varrho BB^T < 0$$

since the above matrix inequality is strict, there exists a sufficiently small $\theta > 0$ for which

$$AP + PA^T - \varrho BB^T + \theta P < 0$$

therefore, the LMIs introduced in the subsequent analysis provide sufficient plant-side feasibility conditions for establishing the stated consensus and tracking results.

Proof The continuous-time Lyapunov test for stabilizability states that stabilizability of (A, B) is equivalent to the existence of a symmetric $P > 0$ satisfying $AP+PA^T-BB^T < 0$. Thus, the first inequality holds with $\varrho = 1$. Let $M = AP + PA^T - \varrho BB^T < 0$ and define $\delta = -\lambda_{\max}(M) > 0$. Since $P > 0$, any $0 < \theta < \delta/\lambda_{\max}(P)$ gives $M + \theta P \le M + \theta\lambda_{\max}(P)I < 0$. Hence the strict LMI with the additional θP term is feasible for a sufficiently small θ. □

On the approximation domain, represent each continuous matched nonlinearity by

$$f_i(x_i(t)) = W_i^T S_i(x_i(t)) + \varepsilon_i(x_i(t)) \quad (2.2)$$

where the basis vector $S_i(x_i(t)) \in \mathbb{R}^p$ is known and bounded by S_{iM}. The ideal coefficient matrix $W_i \in \mathbb{R}^{p\times m}$ is unknown, with $\|W_i\|_F \le W_{iM}$, and the approximation residual satisfies $\|\varepsilon_i(x_i(t))\| \le \varepsilon_{iM}$. The implemented compensator replaces W_i with its online estimate $\hat{W}_i(t)$

$$\hat{f}_i(x_i(t)) = \hat{W}_i^T(t) S_i(x_i(t)) \quad (2.3)$$

for $i = 1, 2, \ldots, N$. Here $\hat{W}_i(t) \in \mathbb{R}^{p\times m}$ is the online estimate of the NN weight matrix.

For concise statement of the gain conditions, define the uniform bounds $\varepsilon_M := \max_{1\le i\le N}\{\varepsilon_{iM}\}, d_M := \max_{1\le i\le N}\{d_{iM}\}$. The norm inequalities imply $\|\varepsilon_i + d_i\|_\infty \le \varepsilon_{iM} + d_{iM}$. Thus, $\varepsilon_M + d_M$ is a uniform componentwise bound for the combined matched residual and disturbance, which can be used directly in the robust-gain conditions.

Assumption 1 *For each admissible initial condition under consideration, every maximal closed-loop Filippov solution has its plant states confined to a prescribed compact set Ω throughout its interval of existence. The representation (2.2) and its uniform bounds hold on this set. In the leader–follower case, the leader state is included among the plant states considered.*

Remark 2 Assumption 1 is a state-domain condition; it does not assume global existence of the closed-loop solution. The Lyapunov estimates apply while the plant states remain in the region where (2.2) is valid. The disagreement Lyapunov function does not establish this property for arbitrary initial conditions or unrestricted nonlinearities. In the leaderless case, it also leaves the common mode unbounded. The constants S_{iM}, W_{iM}, and ε_{iM} are analytical bounds; they are not online signals, and no global bound on f_i is imposed in the general model.

For a candidate set $\Omega_i = \{x_i : \psi_i(x_i) \le 0\}$, with $\psi_i \in C^1$, invariance can be checked by verifying

$$\sup_{\nu\in\mathcal{F}_{\mathrm{cl}}(z)} \nabla\psi_i(x_i)^T \nu_{x_i} \le 0$$

whenever $\psi_i(x_i) = 0$, for every admissible augmented state and disturbance. Here $\mathcal{F}_{\mathrm{cl}}$ is the Filippov flow map of the closed loop, including the adaptive and held variables, and ν_{x_i} is its plant-state component. The tangent condition must hold for every admissible augmented state on the boundary, not just along a simulated path. Since release events do not reset x_i, no jump condition is needed for this constraint. The numerical examples do not prove invariance for a general unknown nonlinearity. Their chosen basis functions

and sinusoidal residuals are globally bounded, however, so the residual bounds used in those examples hold for all states.

Condition 1 *Whenever the NN weights are to be interpreted as learned approximator parameters, the basis-function vector of each agent is assumed to be uniformly persistently exciting. Specifically, for every $i \in \{1, \dots, N\}$, there exist constants $T_{\mathrm{PE}} > 0$ and $\mu_i > 0$ such that*

$$\int_t^{t+T_{\mathrm{PE}}} S_i(x_i(s)) S_i^T(x_i(s))\, \mathrm{d}s \geq \mu_i I_p \qquad (2.4)$$

for all $t \geq 0$. The constants may be chosen agent dependent, a common window T_{PE} is used only to simplify notation.

Remark 3 Condition 1 is not required for either coordination theorem. It is used only to discuss parameter identification. A finite-window Gramian may indicate insufficient excitation over the observed interval, but it does not establish the uniform persistent excitation condition in (2.4). As the agents converge toward a common trajectory, the basis functions may fail to excite certain parameter directions. Consequently, the weights may converge to limits determined by the initial estimates and the resulting trajectory. Moreover, persistent excitation alone does not ensure exact parameter recovery when approximation residuals and disturbances are present. Such a guarantee requires additional assumptions on the identification error or an appropriate prediction-error mechanism. Between consecutive events, the sampled aggregate is held constant, while the remaining states evolve continuously. The signum term is treated in the Filippov sense. Under Assumption 1, the resulting set-valued dynamics have nonempty compact convex values and are locally bounded. The closed-loop solutions are therefore locally absolutely continuous. At each event, the held aggregate is reset, whereas the plant state remains continuous. Hence, the derivative inequalities used below hold almost everywhere along the closed-loop trajectories.

3 Main Results

3.1 Leaderless consensus

Let $\mathcal{G} = (\mathcal{V}, \mathcal{E}, A_{\mathcal{G}})$ be an undirected weighted graph with adjacency matrix $A_{\mathcal{G}} = [a_{ij}]$, degree matrix $D = \mathrm{diag}\{\sum_j a_{ij}\}$, and Laplacian $L = D - A_{\mathcal{G}}$. The neighbor set of agent i is $\mathcal{N}_i = \{j : (j,i) \in \mathcal{E}\}$. The linear coupling uses a held disagreement aggregate, whereas the robust term and adaptation laws use its current value. This allocation determines the sampling-error terms in the Lyapunov analysis. Define the global consensus error $e_i(t) = x_i(t) - \frac{1}{N}\sum_{j=1}^{N} x_j(t)$, which can be written as $e(t) = (\Xi \otimes I_n)x(t)$, where $e(t) = \mathrm{col}(e_1(t), e_2(t), \dots, e_N(t))$, $x(t) = \mathrm{col}(x_1(t), x_2(t), \dots, x_N(t))$, and $\Xi = I_N - \frac{1}{N}\mathbf{1}\mathbf{1}^T$. The matrix Ξ satisfies $L\Xi = \Xi L = L$, which is used repeatedly in the analysis.

The neighborhood error of agent i ($i = 1, 2, \dots, N$) is defined as

$$\delta_i(t) = \sum_{j \in \mathcal{N}_i} a_{ij}\big(x_i(t) - x_j(t)\big) \qquad (3.1)$$

where a_{ij} is the corresponding element of the adjacency matrix.

The aggregate signal in the linear coupling is updated only at release instants and held constant between updates [39]. Let $\{t_k^i\}_{k=0}^{\infty}$ denote the release times of agent i. At each t_k^i, the aggregate buffer is refreshed as follows

$$\hat{\delta}_i(t) = \delta_i(t_k^i) \qquad t \in [t_k^i, t_{k+1}^i) \qquad (3.2)$$

hence $\hat{\delta}_i(t_k^i) = \delta_i(t_k^i)$ and the sampling error $\tilde{\delta}_i(t) = \delta_i(t) - \hat{\delta}_i(t)$ is reset to zero at every event of agent i. The stacked variables are $\delta(t) = \mathrm{col}(\delta_1(t), \dots, \delta_N(t)) = (L \otimes I_n)e(t)$ and $\hat{\delta}(t) = \mathrm{col}(\hat{\delta}_1(t), \dots, \hat{\delta}_N(t))$.

Based on (3.1) and (3.2), the distributed adaptive consensus controller is designed as

$$\begin{aligned} u_i(t) &= \alpha_i(t) F \hat{\delta}_i(t) + \beta_i(t)\, \mathrm{sgn}\big(F\delta_i(t)\big) \\ &\quad - \hat{W}_i^T(t) S_i(x_i(t)) \\ \dot{\alpha}_i(t) &= k_i \delta_i^T(t) \Gamma \hat{\delta}_i(t) e^{\hat{\alpha} t} \\ \dot{\beta}_i(t) &= v_i \big(F\delta_i(t)\big)^T \mathrm{sgn}\big(F\delta_i(t)\big) \\ &\quad - \lambda_\beta\big(\beta_i(t) - \beta_i^\circ\big) \end{aligned} \qquad (3.3)$$

where $\lambda_\beta > 0$ and $\beta_i^\circ > 0$ are prescribed design constants. The quantity β_i° is allowed to be agent dependent and specifies the finite target of the nonsmooth adaptive gain, α_i and β_i weight the linear and nonsmooth feedback terms. The gains F and Γ are fixed.

The neural-network weights are updated according to

$$\begin{aligned} \dot{\hat{W}}_i(t) &= -\tau_i \Big[S_i(x_i(t)) \delta_i^T(t) F^T \\ &\qquad + \sigma_i\big(\hat{W}_i(t) - \bar{W}_i(t)\big) \Big] e^{\hat{r}_1 t} \\ \dot{\bar{W}}_i(t) &= \sigma_i \pi_i \big(\hat{W}_i(t) - \bar{W}_i(t)\big) e^{\hat{r}_2 t} \end{aligned} \qquad (3.4)$$

where $\bar{W}_i$ is an auxiliary weight state. All adaptation-rate parameters in (3.3)–(3.4) are positive.

Remark 4 The update directions in (3.3) cancel the terms involving the unknown adaptive gains in the derivative of the disagreement energy. The leakage term in the β_i law leaves the negative contribution $-2\lambda_\beta(\beta_i - \beta_i^\circ)^2/\upsilon_i$ and drives the robust gain toward its prescribed target. By contrast, the Lyapunov term associated with α_i is exponentially weighted. Without an additional rate condition, it does not by itself imply convergence or uniform boundedness of the unweighted $\alpha_i(t)$. Only the linear coupling uses $\hat{\delta}_i$. The robust feedback, adaptation laws, and trigger use the current aggregate δ_i, which is assumed to be available from local relative sensing or a trusted measurement channel. The numerical count therefore records refreshes of the per-agent aggregate buffer; it does not count the underlying sensor samples, all neighbor-to-neighbor packets, or protocol overhead. If δ_i were reconstructed only from asynchronous neighbor broadcasts, the additional measurement errors and jump dynamics would require a separate analysis. The signal allocation is summarized in Fig. 1.

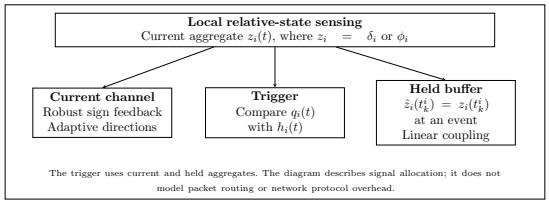


Fig. 1 Information structure of the split-information event-triggered controller

Let $\tilde{\delta}_i(t) = \delta_i(t) - \hat{\delta}_i(t)$ and define

$$q_i(t) = \frac{15}{2}\bar{\alpha}\tilde{\delta}_i^T(t)\Gamma\tilde{\delta}_i(t) - \frac{1}{8}\bar{\alpha}\hat{\delta}_i^T(t)\Gamma\hat{\delta}_i(t)$$
$$h_i(t) = \eta_i(t)e^{-\gamma t}$$

The next event-triggering time of agent i is defined by

$$t_{k+1}^i = \inf\left\{t > t_k^i : q_i(t) > h_i(t)\right\} \tag{3.5}$$

The auxiliary threshold state $\eta_i(t)$ is governed by

$$\dot{\eta}_i(t) = -\rho_i\eta_i(t) - (1-\rho_i)q_i(t)e^{\gamma t} \tag{3.6}$$

where $\eta_i(0) > 0$ and $0 < \rho_i < 1$ are prescribed constants. Thus an event occurs whenever $q_i(t) > h_i(t)$ between consecutive releases.

Lemma 2 *If $\eta_i(0) > 0$, then $\eta_i(t) > 0$ for every finite $t \geq 0$.*

Proof Between consecutive events, $q_i(t) \leq \eta_i(t)e^{-\gamma t}$. Rewriting (3.6) as

$$\dot{\eta}_i(t) = -\rho_i\eta_i(t) - (1-\rho_i)q_i(t)e^{\gamma t}$$

therefore

$$\dot{\eta}_i(t) \geq -\rho_i\eta_i(t) - (1-\rho_i)\eta_i(t) = -\eta_i(t)$$

the comparison lemma yields $\eta_i(t) \geq \eta_i(0)e^{-t} > 0$ on every finite inter-event interval. Since η_i is continuous at triggering instants, the estimate extends to all finite t. □

Remark 5 The effective threshold $h_i(t) = \eta_i(t)e^{-\gamma t}$ satisfies $\dot{h}_i(t) = -(\rho_i + \gamma)h_i(t) - (1-\rho_i)q_i(t)$. Its evolution is coupled to the trigger residual $q_i(t)$ and is therefore not determined by exponential decay alone. Increasing γ raises the explicit decay rate of the threshold. However, the resulting release times also depend on the evolution of the closed-loop disagreement and the hold error [38]. State-dependent event-triggering mechanisms have also been investigated for Euler–Lagrange systems, neural-network-based funnel control, and formation–containment problems subject to communication attacks [15, 16, 25, 26].

A static counterpart can be defined through

$$t_{k+1}^i(\mu) = \inf\{t > t_k^i : q_i(t) > \mu h_i(t)\}$$

here $0 \leq \mu \leq 1$, and the implemented rule uses $\mu = 1$. Setting $\mu = 0$ removes the dynamic slack from the event inequality and gives

$$t_{k+1}^i = \inf\left\{t > t_k^i : q_i(t) > 0\right\} \tag{3.7}$$

this reduction changes the event test only. It should not be interpreted as setting $\eta_i(t) \equiv 0$ in (3.6), since that substitution would generally be inconsistent with the threshold dynamics.

Substituting (2.2) and (3.3) into (2.1) gives

$$\begin{aligned}\dot{x}_i(t) = {} & Ax_i(t) + \alpha_i(t)BF\hat{\delta}_i(t) \\ & +\beta_i(t)B\,\mathrm{sgn}\big(F\delta_i(t)\big) \\ & -B\tilde{W}_i^T(t)S_i(x_i(t)) \\ & +B\varepsilon_i(x_i(t)) + Bd_i(t)\end{aligned} \tag{3.8}$$

where $\tilde{W}_i(t) = \hat{W}_i(t) - W_i$.

Using the stacked sampled aggregate $\hat{\delta}(t)$, (3.8) can be written as

$$\begin{aligned}\dot{x}(t) = {} & (I_N \otimes A)x(t) + (M_1 \otimes BF)\hat{\delta}(t) \\ & +(M_2 \otimes B)\,\mathrm{sgn}\big((I_N \otimes F)\delta(t)\big) \\ & -(I_N \otimes B)\tilde{W}^T(t)S(x(t)) \\ & +(I_N \otimes B)\varepsilon(x(t)) + (I_N \otimes B)d(t)\end{aligned} \tag{3.9}$$

where

$$M_1 = \mathrm{diag}\{\alpha_i(t)\}_{i=1}^N$$

$$
\begin{aligned}
M_2 &= \mathrm{diag}\{\beta_i(t)\}_{i=1}^N \\
\tilde{W}(t) &= \mathrm{diag}\{\tilde{W}_i(t)\}_{i=1}^N \\
S(x(t)) &= \mathrm{col}\{S_i(x_i(t))\}_{i=1}^N \\
\varepsilon(x(t)) &= \mathrm{col}\{\varepsilon_i(x_i(t))\}_{i=1}^N \\
d(t) &= \mathrm{col}\{d_i(t)\}_{i=1}^N
\end{aligned}
$$

Substituting (3.9) into $e(t) = (\Xi \otimes I_n)x(t)$ yields

$$
\begin{aligned}
\dot{e}(t) = {} & (I_N \otimes A)e(t) + (\Xi M_1 \otimes BF)\hat{\delta}(t) \\
& + (\Xi M_2 \otimes B)\,\mathrm{sgn}\big((I_N \otimes F)\delta(t)\big) \\
& - (\Xi \otimes B)\tilde{W}^T(t)S(x(t)) \\
& + (\Xi \otimes B)\varepsilon(x(t)) + (\Xi \otimes B)d(t) \qquad (3.10)
\end{aligned}
$$

where the matrix $\Xi \otimes B$ maps the stacked matched-input terms into the projected error dynamics. In (3.10), the approximation residual and external disturbance enter as additive terms with positive signs. Their effects on the Lyapunov derivative are bounded below.

Theorem 1 *Suppose that the communication graph is undirected and connected and Assumption 1 holds. Let $P = P^T > 0$ satisfy*

$$
AP + PA^T - \varrho BB^T + \theta P < 0 \qquad (3.11)
$$

for some $\varrho, \theta > 0$. Set $F = -B^T P^{-1}$ and $\Gamma = P^{-1}BB^T P^{-1}$, and choose

$$
\begin{aligned}
\bar{\alpha} &> \frac{2\varrho}{\lambda_2(L)} \qquad \lambda_\beta > 0 \\
\underline{\beta}^\circ &= \min_{1\le i\le N} \beta_i^\circ > \varepsilon_M + d_M
\end{aligned}
$$

then for every closed-loop Filippov solution satisfying Assumption 1, the distributed adaptive protocol (3.3), the NN updating law (3.4), the triggering condition (3.5), and the auxiliary dynamics (3.6) achieve complete consensus. More precisely, with

$$
\begin{aligned}
\bar{\theta} &= \min\{\theta, \hat{\alpha}, 2\lambda_\beta, \hat{r}_1, \hat{r}_2, \gamma\} \\
a_1 &= \frac{\lambda_2(L)}{\lambda_{\max}(P)}
\end{aligned}
$$

the disagreement satisfies

$$
\|e(t)\| \le \sqrt{\frac{V(0)}{a_1}}\, e^{-\bar{\theta}t/2} \qquad (t \ge 0) \qquad (3.12)
$$

and therefore

$$
\lim_{t\to\infty} \|x_i(t) - x_j(t)\| = 0 \qquad (i, j = 1, \dots, N)
$$

in addition, the nonsmooth adaptive gains converge exponentially to their prescribed agent-dependent targets

$$
|\beta_i(t) - \beta_i^\circ| \le \sqrt{v_i V(0)}\, e^{-\bar{\theta}t/2}
$$

these estimates are conditional on Assumption 1. Forward completeness follows from the finite-time growth argument and the non-Zeno result, but invariance of Ω remains a separate solution-domain requirement. No convergence claim for the unweighted $\alpha_i(t)$ or NN weights is inferred solely from their exponentially weighted Lyapunov terms. Condition 1 is not needed for complete consensus or for (3.13).

Proof Let $Q = P^{-1} = Q^T > 0$ and introduce the transformed disagreement

$$
\begin{aligned}
\breve{e} &= (I_N \otimes Q)e \\
e &= (I_N \otimes P)\breve{e}
\end{aligned}
$$

since $(\mathbf{1}_N^T \otimes I_n)e = 0$, one also has $(\mathbf{1}_N^T \otimes I_n)\breve{e} = 0$. Hence $\breve{e}$ belongs to the disagreement subspace of the undirected Laplacian L.

Consider the composite Lyapunov function

$$
V(t) = V_1(t) + V_2(t) + V_3(t) + V_4(t) \qquad (3.13)
$$

where

$$
V_1 = e^T(L \otimes Q)e \qquad (3.14)
$$

$$
V_2 = \sum_{i=1}^N \frac{(\alpha_i - \bar{\alpha})^2}{k_i} e^{-\hat{\alpha}t} + \sum_{i=1}^N \frac{(\beta_i - \beta_i^\circ)^2}{v_i} \qquad (3.15)
$$

$$
V_3 = \sum_{i=1}^N \frac{\|\tilde{W}_i\|_F^2}{\tau_i} e^{-\hat{r}_1 t} + \sum_{i=1}^N \frac{\|\hat{\tilde{W}}_i\|_F^2}{\pi_i} e^{-\hat{r}_2 t} \qquad (3.16)
$$

$$
V_4 = \sum_{i=1}^N \eta_i e^{-\gamma t} \qquad (3.17)
$$

where $\tilde{W}_i = \hat{W}_i - W_i$ and $\hat{\tilde{W}}_i = \bar{W}_i - W_i$. By Lemma 2, $V_4 > 0$ for every finite time, while the other terms are nonnegative.

Because $L = L^T$, $L\Xi = L$, $\delta = (L \otimes I_n)e$, and $QB = -F^T$, differentiating V_1 along (3.10) gives, almost everywhere along a Filippov solution

$$
\begin{aligned}
\dot{V}_1 = {} & e^T\Big[L \otimes (QA + A^TQ)\Big]e - 2\sum_{i=1}^N \alpha_i \delta_i^T \Gamma \hat{\delta}_i \\
& - 2\sum_{i=1}^N \beta_i (F\delta_i)^T \,\mathrm{sgn}(F\delta_i) \\
& + 2\sum_{i=1}^N (F\delta_i)^T \tilde{W}_i^T S_i \\
& + 2e^T(L \otimes QB)(\varepsilon + d) \qquad (3.18)
\end{aligned}
$$

where $(F\delta_i)^T \,\mathrm{sgn}(F\delta_i) = \|F\delta_i\|_1, \Gamma = QBB^TQ = F^TF$. Moreover

$$
e^T[L \otimes (QA + A^TQ)]e = \breve{e}^T[L \otimes (AP + PA^T)]\breve{e} \qquad (3.19)
$$

From (3.3), we can obtain

$$
\dot{V}_2 = 2\sum_{i=1}^N (\alpha_i - \bar{\alpha})\delta_i^T \Gamma \hat{\delta}_i
$$

$$+2\sum_{i=1}^{N}(\beta_i-\beta_i^\circ)(F\delta_i)^T\operatorname{sgn}(F\delta_i)$$
$$-\hat{\alpha}\sum_{i=1}^{N}\frac{(\alpha_i-\bar{\alpha})^2}{k_i}e^{-\hat{\alpha}t}$$
$$-2\lambda_\beta\sum_{i=1}^{N}\frac{(\beta_i-\beta_i^\circ)^2}{v_i} \tag{3.20}$$

therefore, the terms containing the unknown instantaneous values α_i and β_i in $\dot{V}_1+\dot{V}_2$ reduce exactly to

$$\begin{aligned}&-2\sum_{i=1}^{N}\alpha_i\delta_i^T\Gamma\hat{\delta}_i+2\sum_{i=1}^{N}(\alpha_i-\bar{\alpha})\delta_i^T\Gamma\hat{\delta}_i\\ =\;&-2\bar{\alpha}\sum_{i=1}^{N}\delta_i^T\Gamma\hat{\delta}_i \qquad (3.21)\\ &-2\sum_{i=1}^{N}\beta_i\|F\delta_i\|_1+2\sum_{i=1}^{N}(\beta_i-\beta_i^\circ)\|F\delta_i\|_1\\ =\;&-2\sum_{i=1}^{N}\beta_i^\circ\|F\delta_i\|_1 \qquad (3.22)\end{aligned}$$

Using (3.4) and the fact that the ideal weights W_i are constant, then

$$\begin{aligned}&\frac{d}{dt}\left(\frac{\|\tilde{W}_i\|_F^2}{\tau_i}e^{-\hat{r}_1t}\right)\\ =\;&-2(F\delta_i)^T\tilde{W}_i^TS_i-2\sigma_i\operatorname{tr}\left[\tilde{W}_i^T(\tilde{W}_i-\hat{\tilde{W}}_i)\right]\\ &-\hat{r}_1\frac{\|\tilde{W}_i\|_F^2}{\tau_i}e^{-\hat{r}_1t} \qquad (3.23)\\ &\frac{d}{dt}\left(\frac{\|\hat{\tilde{W}}_i\|_F^2}{\pi_i}e^{-\hat{r}_2t}\right)\\ =\;&2\sigma_i\operatorname{tr}\left[\hat{\tilde{W}}_i^T\tilde{W}_i\right]-2\sigma_i\|\hat{\tilde{W}}_i\|_F^2\\ &-\hat{r}_2\frac{\|\hat{\tilde{W}}_i\|_F^2}{\pi_i}e^{-\hat{r}_2t} \qquad (3.24)\end{aligned}$$

The two σ_i-terms satisfy

$$\begin{aligned}&-2\sigma_i\|\tilde{W}_i\|_F^2-2\sigma_i\|\hat{\tilde{W}}_i\|_F^2+4\sigma_i\operatorname{tr}(\tilde{W}_i^T\hat{\tilde{W}}_i)\\ &\qquad=-2\sigma_i\|\tilde{W}_i-\hat{\tilde{W}}_i\|_F^2\le 0\end{aligned}$$

Consequently, the first term in (3.23) cancels the NN cross term in (3.18), one has

$$\begin{aligned}&\dot{V}_1+\dot{V}_2+\dot{V}_3\\ \le\;&\breve{e}^T[L\otimes(AP+PA^T)]\breve{e}-2\bar{\alpha}\,\delta^T(I_N\otimes\Gamma)\hat{\delta}\\ &-2\sum_{i=1}^{N}\beta_i^\circ\|F\delta_i\|_1+2e^T(L\otimes QB)(\varepsilon+d)\\ &-\hat{\alpha}V_{2\alpha}-2\lambda_\beta V_{2\beta}-\hat{r}_1V_{3a}-\hat{r}_2V_{3b} \qquad (3.25)\end{aligned}$$

where $V_{2\alpha},V_{2\beta},V_{3a},V_{3b}$ denote the four nonnegative summands in (3.15)–(3.16).

Since $\hat{\delta}=\delta-\tilde{\delta}$, one can obtain

$$\begin{aligned}&-2\bar{\alpha}\,\delta^T(I_N\otimes\Gamma)\hat{\delta}\\ =\;&-\frac{1}{2}\bar{\alpha}\,\delta^T(I_N\otimes\Gamma)\delta-\frac{3}{2}\bar{\alpha}\,\delta^T(I_N\otimes\Gamma)\delta\\ &+2\bar{\alpha}\,\delta^T(I_N\otimes\Gamma)\tilde{\delta} \qquad (3.26)\end{aligned}$$

because $\delta=(L\otimes I_n)e$ and $e=(I_N\otimes P)\breve{e}$, one obtains $\delta^T(I_N\otimes\Gamma)\delta=\breve{e}^T(L^2\otimes BB^T)\breve{e}$. For every vector in the disagreement subspace

$$\breve{e}^T(L^2\otimes BB^T)\breve{e}\ge\lambda_2(L)\,\breve{e}^T(L\otimes BB^T)\breve{e} \tag{3.27}$$

indeed, (3.27) follows by diagonalizing the symmetric Laplacian and using $\lambda_j^2(L)\ge\lambda_2(L)\lambda_j(L)$ for $j=2,\dots,N$. Hence, from $\bar{\alpha}\lambda_2(L)/2>\varrho$ and (3.11), define $\mathcal{M}_1=AP+PA^T-\frac{1}{2}\bar{\alpha}\lambda_2(L)BB^T$, then

$$\begin{aligned}&\breve{e}^T\left[L\otimes(AP+PA^T)-\frac{1}{2}\bar{\alpha}(L^2\otimes BB^T)\right]\breve{e}\\ &\le\breve{e}^T[L\otimes\mathcal{M}_1]\breve{e}\\ &\le\breve{e}^T[L\otimes(AP+PA^T-\varrho BB^T)]\breve{e}\\ &\le-\theta\,\breve{e}^T(L\otimes P)\breve{e}=-\theta V_1 \qquad (3.28)\end{aligned}$$

It remains to estimate the second line of (3.26). Using $\delta=\hat{\delta}+\tilde{\delta}$, one has

$$\begin{aligned}&-\frac{3}{2}\delta^T(I_N\otimes\Gamma)\delta+2\delta^T(I_N\otimes\Gamma)\tilde{\delta}\\ &=-\frac{3}{2}\hat{\delta}^T(I_N\otimes\Gamma)\hat{\delta}-\hat{\delta}^T(I_N\otimes\Gamma)\tilde{\delta}\\ &\quad+\frac{1}{2}\tilde{\delta}^T(I_N\otimes\Gamma)\tilde{\delta} \qquad (3.29)\end{aligned}$$

Since $\Gamma\ge0$, by using Young's inequality, we can obtain

$$-\hat{\delta}^T(I_N\otimes\Gamma)\tilde{\delta}\le\frac{1}{2}\hat{\delta}^T(I_N\otimes\Gamma)\hat{\delta}+\frac{1}{2}\tilde{\delta}^T(I_N\otimes\Gamma)\tilde{\delta}$$

thus

$$\begin{aligned}&-\tfrac{3}{2}\delta^T(I_N\otimes\Gamma)\delta+2\delta^T(I_N\otimes\Gamma)\tilde{\delta}\\ &\le-\hat{\delta}^T(I_N\otimes\Gamma)\hat{\delta}+\tilde{\delta}^T(I_N\otimes\Gamma)\tilde{\delta}.\end{aligned}$$

For compatibility with the prescribed trigger, the right-hand side is conservatively relaxed as

$$\begin{aligned}&-\hat{\delta}^T(I_N\otimes\Gamma)\hat{\delta}+\tilde{\delta}^T(I_N\otimes\Gamma)\tilde{\delta}\\ \le\;&-\frac{1}{8}\hat{\delta}^T(I_N\otimes\Gamma)\hat{\delta}+\frac{15}{2}\tilde{\delta}^T(I_N\otimes\Gamma)\tilde{\delta} \qquad (3.30)\end{aligned}$$

Recall the uniform bounds ε_M and d_M defined in Section 2, and set $c_1=\varepsilon_M+d_M$. Since $QB=-F^T$ and $\delta=(L\otimes I_n)e$, then

$$\begin{aligned}&2e^T(L\otimes QB)(\varepsilon+d)\\ =\;&-2\sum_{i=1}^{N}(F\delta_i)^T(\varepsilon_i+d_i)\le2c_1\sum_{i=1}^{N}\|F\delta_i\|_1\\ =\;&2c_1\|(I_N\otimes F)\delta\|_1 \qquad (3.31)\end{aligned}$$

Therefore, with $\underline{\beta}^\circ = \min_i \beta_i^\circ$, one has

$$\begin{aligned}
&-2\sum_{i=1}^{N}\beta_i^\circ\|F\delta_i\|_1 + 2e^T(L\otimes QB)(\varepsilon+d)\\
&\le -2\sum_{i=1}^{N}(\beta_i^\circ - c_1)\|F\delta_i\|_1\\
&\le -2(\underline{\beta}^\circ - c_1)\|(I_N\otimes F)\delta\|_1 \le 0
\end{aligned} \tag{3.32}$$

Combining (3.28), (3.30), and (3.32) with (3.25) yields

$$\begin{aligned}
\sum_{j=1}^{3}\dot V_j \;\le\; &-\theta V_1 + \sum_{i=1}^{N} q_i - \hat\alpha V_{2\alpha} - 2\lambda_\beta V_{2\beta}\\
&-\hat r_1 V_{3a} - \hat r_2 V_{3b}
\end{aligned} \tag{3.33}$$

where $q_i = \frac{15}{2}\bar\alpha\tilde\delta_i^T\Gamma\tilde\delta_i - \frac{1}{8}\bar\alpha\hat\delta_i^T\Gamma\hat\delta_i$.

Set $h_i = \eta_i e^{-\gamma t}$, it can be obtained from (3.6) that

$$\dot\eta_i = -\rho_i\eta_i - (1-\rho_i)q_i e^{\gamma t}$$

Therefore

$$\dot V_4 \;=\; \sum_{i=1}^{N} e^{-\gamma t}(\dot\eta_i - \gamma\eta_i) = -\sum_{i=1}^{N}(\rho_i+\gamma)h_i \tag{3.34}$$

Between consecutive events, (3.5) gives $q_i \le h_i$. Hence

$$\begin{aligned}
\sum_{i=1}^{N} q_i + \dot V_4 \;&=\; \sum_{i=1}^{N}\rho_i(q_i - h_i)\\
&-\gamma\sum_{i=1}^{N} h_i \le -\gamma V_4
\end{aligned} \tag{3.35}$$

Finally, from (3.33) and (3.35), one has

$$\begin{aligned}
\dot V \;&\le\; -\theta V_1 - \hat\alpha V_{2\alpha} - 2\lambda_\beta V_{2\beta}\\
&\quad -\hat r_1 V_{3a} - \hat r_2 V_{3b} - \gamma V_4\\
&\le\; -\bar\theta V
\end{aligned} \tag{3.36}$$

where $\bar\theta = \min\{\theta, \hat\alpha, 2\lambda_\beta, \hat r_1, \hat r_2, \gamma\}$.

Since the inequality holds almost everywhere, integration along the absolutely continuous Filippov solution yields

$$V(t) \;\le\; V(0)e^{-\bar\theta t} \tag{3.37}$$

Since e lies in the disagreement subspace, one has

$$\begin{aligned}
V_1 \;&=\; e^T(L\otimes Q)e \ge \lambda_2(L)\lambda_{\min}(Q)\|e\|^2\\
&=\; \frac{\lambda_2(L)}{\lambda_{\max}(P)}\|e\|^2 = a_1\|e\|^2
\end{aligned} \tag{3.38}$$

Consequently

$$\|e(t)\| \le \sqrt{\tfrac{V(0)}{a_1}}\, e^{-\bar\theta t/2}$$

Moreover, $V_{2\beta} \le V$ gives

$$\tfrac{(\beta_i(t)-\beta_i^\circ)^2}{v_i} \le V(t) \le V(0)e^{-\bar\theta t}$$

which proves (3.13). Finally, $x_i - x_j = e_i - e_j$ and $\|e_i - e_j\| \le \sqrt{2}\,\|e\|$, so $\|x_i(t) - x_j(t)\| \to 0$ for all i, j. This establishes complete consensus and convergence of each nonsmooth adaptive gain to its prescribed target. □

Corollary 1 *Under Theorem 1,*

$$\|e(t)\| \;\le\; \sqrt{\frac{V(0)}{a_1}}\, e^{-\bar\theta t/2} \tag{3.39}$$

for any prescribed $r > 0$, a conservative entrance time into $\|e\| \le r$ is

$$T_r \;=\; \max\left\{0, \frac{1}{\bar\theta}\ln\frac{V(0)}{a_1 r^2}\right\} \tag{3.40}$$

Remark 6 Using the current aggregate in the robust feedback is crucial for achieving exact consensus. It enables the nonsmooth term to compensate for bounded disturbances and approximation residuals without introducing a nonzero consensus error bound. By contrast, the held aggregate appears only in the linear coupling, and its mismatch is accounted for by the event-triggering mechanism. The gain requirement $\bar\alpha > 2\varrho/\lambda_2(L)$ depends explicitly on the algebraic connectivity of the communication graph. Hence, although the controller operates on local signals, selecting a gain that satisfies the theoretical condition requires graph-level information. The LMI (3.11) provides a sufficient condition on the plant parameters, with its feasibility linked to stabilizability through Lemma 1. In implementation, the plant certificate, graph margin, and triggering parameters should be selected jointly, since their interaction influences both the convergence estimate and the frequency of release events.

Theorem 2 *Under Assumption 1, the aggregate reset convention (3.2), and the leaderless event-triggering condition (3.5), no triggering sequence of an individual agent can accumulate in finite time.*

Proof Assume, to the contrary, that the events of some agent i accumulate at a finite time T. By Lemma 2, we can obtain

$$h_i(t) \;=\; \eta_i(t)e^{-\gamma t} \ge \eta_i(0)e^{-(1+\gamma)T} =: h_{i,T} > 0$$

for $0 \le t < T$.

At each event, (3.2) gives $\tilde\delta_i(t_k^i) = 0$. Hence the trigger residual immediately after reset satisfies

$$q_i(t_k^i) = -\tfrac{1}{8}\bar\alpha\hat\delta_i^T(t_k^i)\Gamma\hat\delta_i(t_k^i) \le 0$$

and therefore the trigger function $g_i(t) = q_i(t) - h_i(t)$ obeys $g_i(t_k^i) \le -h_{i,T} < 0$.

On the finite interval $[0, T)$, all exponential multipliers in the adaptive laws are uniformly bounded. Assumption 1 keeps the state in the compact approximation domain, so $S_i(x_i)$, the approximation residuals, and the local disagreement signals remain bounded; the external disturbances are bounded by the standing hypothesis in (2.1). The adaptive weight dynamics are affine in the weight variables with bounded coefficients and bounded forcing terms on $[0, T)$, and Grönwall's inequality therefore gives finite bounds for $\hat W_i$ and $\bar W_i$.

The scalar adaptive-gain equations yield finite bounds for α_i and β_i in the same way.

Because the Filippov vector field is bounded on this finite closed-loop region, the plant trajectory is absolutely continuous. In fact, Lipschitz on each compact subinterval of $[0, T)$. Hence δ_i is absolutely continuous with an essentially bounded derivative between resets. The held value $\hat{\delta}_i$ is constant on each open inter-event interval, so q_i, h_i, and $g_i = q_i - h_i$ are absolutely continuous there. Consequently, there exists $M_{i,T} > 0$ such that

$$|\dot{g}_i(t)| \le M_{i,T}$$

for almost every $t \in [t_k^i, t_{k+1}^i) \cap [0, T)$.

Integrating this a.e. bound gives

$$g_i(t) - g_i(t_k^i) \le M_{i,T}(t - t_k^i)$$

Since $g_i(t_k^i) \le -h_{i,T}$, reaching the trigger surface $g_i = 0$ requires

$$t_{k+1}^i - t_k^i \ge \tfrac{h_{i,T}}{M_{i,T}} > 0$$

thus every event sequence has a uniform positive dwell time on $[0, T)$, contradicting finite-time accumulation. Zeno behavior is therefore excluded for the leaderless design. □

Remark 7 (Continuation of maximal solutions) The compact-state condition in Assumption 1 bounds the plant states on every finite interval of existence. On such an interval, the basis functions and disturbances are bounded, and the adaptive differential equations have at most linear growth in the adaptive variables, with coefficients that remain bounded on finite time intervals. Grönwall's inequality therefore rules out finite-time blow-up of the adaptive states. The positive inter-event lower bound established above rules out finite-time accumulation of resets. Together with local existence of the Filippov flow, these facts permit continuation of every maximal solution and hence give forward completeness under Assumption 1. This establishes forward completeness for the leaderless design under Assumption 1.

3.2 Leader–follower tracking

For leader–follower tracking, the same information split is used, and the bounded leader input enters the tracking-error dynamics as an additional matched signal. The follower and leader dynamics are given as

$$\begin{aligned}\dot{x}_i(t) &= Ax_i(t) + B[u_i(t) + f_i(x_i(t)) \\ &\quad + d_i(t)] \qquad (3.41)\\ \dot{x}_{N+1}(t) &= Ax_{N+1}(t) + Bu_{N+1}(t) \qquad (3.42)\end{aligned}$$

for $i = 1, 2, \ldots, N$, where x_{N+1} and u_{N+1} denote the leader state and input, respectively, with $\|u_{N+1}(t)\|_\infty \le \kappa$ almost everywhere. The pair (A, B) is stabilizable. The objective is to drive each follower error $x_i - x_{N+1}$ to zero despite the matched uncertainty, bounded disturbances, and intermittent aggregate updates.

Assumption 2 *The follower graph is undirected and connected, and at least one follower can directly receive information from the leader.*

Let $\bar{G} = (\bar{V}, \bar{E}, \bar{A})$ be a weighted graph composed of N followers and one leader. Under Assumption 2, its Laplacian matrix can be partitioned as

$$\bar{L} = \begin{bmatrix} L_1 & -\bar{a} \\ 0_N^T & 0 \end{bmatrix} \qquad (3.43)$$

where $\bar{a} = \mathrm{col}(\bar{a}_{1,N+1}, \bar{a}_{2,N+1}, \ldots, \bar{a}_{N,N+1})$ as the leader–follower pinning-weight vector and set $L_1 = L + \mathrm{diag}\{\bar{a}\}$. Because the follower graph is undirected and connected and at least one pinning weight is positive, L_1 is symmetric positive definite.

For the leader–follower formulation, the tracking error $\varphi_i(t)$ and the local tracking error $\phi_i(t)$ are introduced as

$$\varphi_i(t) = x_i(t) - x_{N+1}(t) \qquad (3.44)$$

$$\phi_i(t) = \sum_{j=1}^{N+1} \bar{a}_{ij}\big(x_i(t) - x_j(t)\big) \qquad (3.45)$$

Lemma 3 *Define the stacked vectors*

$$\begin{aligned}x(t) &= \mathrm{col}(x_1(t), \ldots, x_N(t))\\ \varphi(t) &= \mathrm{col}(\varphi_1(t), \ldots, \varphi_N(t))\\ \phi(t) &= \mathrm{col}(\phi_1(t), \ldots, \phi_N(t))\end{aligned}$$

then we have $\phi(t) = (L_1 \otimes I_n)\varphi(t)$ *with* L_1 *defined in* (3.43).

Proof From the definitions of $\bar{L}$ and $\phi(t)$, we can obtain

$$\begin{bmatrix} \phi(t) \\ \phi_{N+1}(t) \end{bmatrix} = \left(\begin{bmatrix} L_1 & -\bar{a} \\ 0_N^T & 0 \end{bmatrix} \otimes I_n \right) \begin{bmatrix} x(t) \\ x_{N+1}(t) \end{bmatrix} \qquad (3.46)$$

therefore

$$\phi(t) = (L_1 \otimes I_n)x(t) - (\bar{a} \otimes I_n)x_{N+1}(t) \qquad (3.47)$$

Using $\varphi_i(t) = x_i(t) - x_{N+1}(t)$ gives

$$x(t) = \varphi(t) + \mathbf{1}_N \otimes x_{N+1}(t) \qquad (3.48)$$

Substituting (3.48) into (3.47) yields

$$\begin{aligned}\phi(t) &= (L_1 \otimes I_n)\varphi(t)\\ &\quad + \big[(L_1\mathbf{1}_N - \bar{a}) \otimes I_n\big]x_{N+1}(t)\\ &= (L_1 \otimes I_n)\varphi(t)\end{aligned}$$

because $L_1\mathbf{1}_N = \bar{a}$. The stated result follows. □

The same aggregate-buffer refresh mechanism is used for leader–follower tracking. Let $t_0^i, t_1^i, \dots$ be the triggering instants of follower i. In parallel with (3.2), the locally measurable aggregate tracking disagreement is sampled and held as

$$\hat{\phi}_i(t) = \phi_i(t_k^i) \qquad t \in [t_k^i, t_{k+1}^i)$$

consequently, $\tilde{\phi}_i(t) = \phi_i(t) - \hat{\phi}_i(t)$ satisfies $\tilde{\phi}_i(t_k^i) = 0$ at each follower event. The stacked sampled variable is $\hat{\phi}(t) = \mathrm{col}(\hat{\phi}_1(t), \dots, \hat{\phi}_N(t))$.

Combining (3.45) and (3.49), the follower controller is designed as

$$\begin{aligned} u_i(t) &= \alpha_i(t) F \hat{\phi}_i(t) + \beta_i(t) \operatorname{sgn}\big(F\phi_i(t)\big) \\ &\quad - \hat{W}_i^T(t) S_i(x_i(t)) \\ \dot{\alpha}_i(t) &= k_i \phi_i^T(t) \Gamma \hat{\phi}_i(t) e^{\hat{\alpha} t} \\ \dot{\beta}_i(t) &= v_i \big(F\phi_i(t)\big)^T \operatorname{sgn}\big(F\phi_i(t)\big) e^{\hat{\beta} t} \end{aligned} \tag{3.49}$$

and the NN adaptive laws are

$$\begin{aligned} \dot{\hat{W}}_i(t) &= -\tau_i \Big[S_i(x_i(t)) \phi_i^T(t) F^T \\ &\qquad + \sigma_i \big(\hat{W}_i(t) - \bar{W}_i(t) \big) \Big] e^{\hat{r}_1 t} \\ \dot{\bar{W}}_i(t) &= \sigma_i \pi_i \big(\hat{W}_i(t) - \bar{W}_i(t) \big) e^{\hat{r}_2 t} \end{aligned} \tag{3.50}$$

where the gains α_i and β_i scale the linear and nonsmooth feedback terms, respectively; $\bar{W}_i$ is the auxiliary neural-weight state. The update directions are chosen to cancel the adaptive-gain cross terms in the tracking-energy derivative. Since the associated Lyapunov terms are exponentially weighted, boundedness of those terms alone does not imply uniform boundedness of the unweighted adaptive gains.

Define the leader–follower trigger residual

$$\begin{aligned} q_i^L(t) &= \frac{57}{7} \bar{\alpha} \tilde{\phi}_i^T(t) \Gamma \tilde{\phi}_i(t) \\ &\quad - \frac{2}{7} \bar{\alpha} \hat{\phi}_i^T(t) \Gamma \hat{\phi}_i(t) \end{aligned} \tag{3.51}$$

where $\tilde{\phi}_i(t) = \phi_i(t) - \hat{\phi}_i(t)$. The event-triggering instants are then recursively specified by

$$t_{k+1}^i = \inf \big\{ t > t_k^i : q_i^L(t) > \eta_i(t) e^{-\gamma t} \big\} \tag{3.52}$$

The auxiliary variable $\eta_i(t)$ satisfies

$$\dot{\eta}_i(t) = -\rho_i \eta_i(t) - (1 - \rho_i) q_i^L(t) e^{\gamma t} \tag{3.53}$$

where $\eta_i(0) > 0$ and $0 < \rho_i < 1$ are prescribed constants.

Between events, $q_i^L(t) \le \eta_i(t) e^{-\gamma t}$. Repeating the comparison argument of Lemma 2 gives

$$\dot{\eta}_i(t) \ge -\eta_i(t)$$

then

$$\eta_i(t) \ge \eta_i(0) e^{-t} > 0$$

for every finite t. Thus the leader–follower dynamic threshold is also strictly positive. The exact static counterpart is obtained at the design level by replacing the inequality $q_i^L(t) > \eta_i(t) e^{-\gamma t}$ with $q_i^L(t) > 0$. The auxiliary dynamics are not used in this static event test.

Substituting (3.49) into (3.41) gives

$$\begin{aligned} \dot{\varphi}_i(t) &= A\varphi_i(t) + \alpha_i(t) B F \hat{\phi}_i(t) \\ &\quad + \beta_i(t) B \operatorname{sgn}\big(F\phi_i(t)\big) \\ &\quad - B \tilde{W}_i^T(t) S_i(x_i(t)) \\ &\quad + B\varepsilon_i(x_i(t)) + B d_i(t) \\ &\quad - B u_{N+1}(t) \end{aligned} \tag{3.54}$$

where $\tilde{W}_i(t) = \hat{W}_i(t) - W_i$. Using the stacked sampled aggregate $\hat{\phi}(t)$, (3.54) can be written compactly as follows

$$\begin{aligned} \dot{\varphi}(t) &= (I_N \otimes A)\varphi(t) + (M_1 \otimes BF)\hat{\phi}(t) \\ &\quad + (M_2 \otimes B) \operatorname{sgn}\big((I_N \otimes F)\phi(t)\big) \\ &\quad - (I_N \otimes B)\tilde{W}^T(t) S(x(t)) \\ &\quad - (I_N \otimes B)\big(\mathbf{1}_N \otimes u_{N+1}(t) \\ &\quad - \varepsilon(x(t)) - d(t)\big) \end{aligned} \tag{3.55}$$

Theorem 3 *Under Assumptions 1 and 2, let $L_1 = L + \mathrm{diag}\{\bar{a}\} > 0$. Let $P = P^T > 0$ satisfy*

$$AP + PA^T - \varrho B B^T + \theta P < 0 \tag{3.56}$$

for some $\varrho, \theta > 0$, and set

$$F = -B^T P^{-1} \qquad \Gamma = P^{-1} B B^T P^{-1}$$

If

$$\bar{\alpha} > \frac{7\varrho}{2\lambda_{\min}(L_1)} \qquad \bar{\beta} > \kappa + \varepsilon_M + d_M$$

then, for every closed-loop Filippov solution satisfying Assumption 1, the controller (3.49), the NN law (3.50), the event-triggered mechanism (3.52), and the auxiliary update law (3.53) achieve exact asymptotic leader tracking. Let

$$\begin{aligned} \bar{\theta} &= \min\{\theta, \hat{\alpha}, \hat{\beta}, \hat{r}_1, \hat{r}_2, \gamma\} \\ a_2 &= \frac{\lambda_{\min}(L_1)}{\lambda_{\max}(P)} \end{aligned}$$

then

$$\|\varphi(t)\| \le \sqrt{\frac{V(0)}{a_2}} e^{-\bar{\theta} t/2} \qquad (t \ge 0) \tag{3.57}$$

and consequently

$$\lim_{t \to \infty} \|x_i(t) - x_{N+1}(t)\| = 0$$

for $i = 1, \dots, N$.

Condition 1 is not required for this tracking conclusion. The estimate is conditional on Assumption 1. Forward completeness follows from the finite-time growth and non-Zeno arguments, whereas invariance of Ω remains a separate solution-domain requirement. The theorem does not assert convergence or uniform boundedness of the unweighted adaptive gains or NN-weight states.

Proof Let $Q = P^{-1}$ and define

$$\breve{\varphi} = (I_N \otimes Q)\varphi$$
$$\varphi = (I_N \otimes P)\breve{\varphi}$$

Since $L_1 = L_1^T > 0$, the tracking energy below is positive definite in φ.

Consider

$$V(t) = V_1(t) + V_2(t) + V_3(t) + V_4(t) \tag{3.58}$$

where

$$V_1 = \varphi^T (L_1 \otimes Q)\varphi \tag{3.59}$$

$$V_2 = \sum_{i=1}^{N} \frac{(\alpha_i - \bar{\alpha})^2}{k_i} e^{-\hat{\alpha}t} + \sum_{i=1}^{N} \frac{(\beta_i - \bar{\beta})^2}{v_i} e^{-\hat{\beta}t} \tag{3.60}$$

$$V_3 = \sum_{i=1}^{N} \frac{\|\tilde{W}_i\|_F^2}{\tau_i} e^{-\hat{r}_1 t} + \sum_{i=1}^{N} \frac{\|\hat{\tilde{W}}_i\|_F^2}{\pi_i} e^{-\hat{r}_2 t} \tag{3.61}$$

$$V_4 = \sum_{i=1}^{N} \eta_i e^{-\gamma t} \tag{3.62}$$

Using $\phi = (L_1 \otimes I_n)\varphi$, $QB = -F^T$, and the tracking dynamics (3.55), one obtains

$$\begin{aligned}\dot{V}_1 = {} & \varphi^T [L_1 \otimes (QA + A^T Q)]\varphi - 2\sum_{i=1}^{N} \alpha_i \phi_i^T \Gamma \hat{\phi}_i \\ & -2\sum_{i=1}^{N} \beta_i (F\phi_i)^T \operatorname{sgn}(F\phi_i) + 2\sum_{i=1}^{N} (F\phi_i)^T \tilde{W}_i^T S_i \\ & -2\varphi^T (L_1 \otimes QB)(\mathbf{1}_N \otimes u_{N+1} - \varepsilon - d)\end{aligned} \tag{3.63}$$

For compactness, let $\mathcal{A}_Q = QA + A^T Q$ and $\mathcal{A}_P = AP + PA^T$. The plant term can then be written in the Q-coordinates as

$$\varphi^T (L_1 \otimes \mathcal{A}_Q)\varphi = \breve{\varphi}^T (L_1 \otimes \mathcal{A}_P)\breve{\varphi} \tag{3.64}$$

Differentiation of V_2 along with (3.49), we have

$$\begin{aligned}\dot{V}_2 = {} & 2\sum_{i=1}^{N} (\alpha_i - \bar{\alpha}) \phi_i^T \Gamma \hat{\phi}_i \\ & +2\sum_{i=1}^{N} (\beta_i - \bar{\beta})(F\phi_i)^T \operatorname{sgn}(F\phi_i) \\ & -\hat{\alpha} V_{2\alpha} - \hat{\beta} V_{2\beta}\end{aligned} \tag{3.65}$$

Thus

$$\begin{aligned}& -2\sum_i \alpha_i \phi_i^T \Gamma \hat{\phi}_i + 2\sum_i (\alpha_i - \bar{\alpha}) \phi_i^T \Gamma \hat{\phi}_i \\ = {} & -2\bar{\alpha} \sum_i \phi_i^T \Gamma \hat{\phi}_i \\ & -2\sum_i \beta_i \|F\phi_i\|_1 + 2\sum_i (\beta_i - \bar{\beta})\|F\phi_i\|_1 \\ = {} & -2\bar{\beta}\|(I_N \otimes F)\phi\|_1\end{aligned} \tag{3.66, 3.67}$$

The derivative of V_3 is identical in structure to (3.23)–(3.24), with δ_i replaced by ϕ_i. Hence the term $2(F\phi_i)^T \tilde{W}_i^T S_i$ is cancelled, while $-2\sigma_i \|\tilde{W}_i - \hat{\tilde{W}}_i\|_F^2 \le 0$ can be dropped from the upper bound. Consequently

$$\begin{aligned}& \dot{V}_1 + \dot{V}_2 + \dot{V}_3 \\ \le {} & \breve{\varphi}^T [L_1 \otimes (AP + PA^T)]\breve{\varphi} - 2\bar{\alpha}\, \phi^T (I_N \otimes \Gamma)\hat{\phi} \\ & -2\bar{\beta}\|(I_N \otimes F)\phi\|_1 - 2\varphi^T (L_1 \otimes QB) \\ & \cdot(\mathbf{1}_N \otimes u_{N+1} - \varepsilon - d) - \hat{\alpha} V_{2\alpha} - \hat{\beta} V_{2\beta} \\ & -\hat{r}_1 V_{3a} - \hat{r}_2 V_{3b}.\end{aligned} \tag{3.68}$$

Since $\hat{\phi} = \phi - \tilde{\phi}$, we have

$$\begin{aligned}& -2\bar{\alpha}\, \phi^T (I_N \otimes \Gamma)\hat{\phi} \\ = {} & -\frac{2}{7}\bar{\alpha}\, \phi^T (I_N \otimes \Gamma)\phi - \frac{12}{7}\bar{\alpha}\, \phi^T (I_N \otimes \Gamma)\phi \\ & +2\bar{\alpha}\, \phi^T (I_N \otimes \Gamma)\tilde{\phi}\end{aligned} \tag{3.69}$$

Because $\phi = (L_1 \otimes I_n)\varphi$, one has

$$\phi^T (I_N \otimes \Gamma)\phi = \breve{\varphi}^T (L_1^2 \otimes BB^T)\breve{\varphi}$$

As $L_1 > 0$ is symmetric, then

$$\begin{aligned}& \breve{\varphi}^T (L_1^2 \otimes BB^T)\breve{\varphi} \\ \ge {} & \lambda_{\min}(L_1) \times \breve{\varphi}^T (L_1 \otimes BB^T)\breve{\varphi}\end{aligned} \tag{3.70}$$

The gain condition $2\bar{\alpha}\lambda_{\min}(L_1)/7 > \varrho$ and the LMI (3.56) therefore imply, with $\mathcal{M}_2 = AP + PA^T - \frac{2}{7}\bar{\alpha}\lambda_{\min}(L_1)BB^T$,

$$\begin{aligned}& \breve{\varphi}^T \left[L_1 \otimes (AP + PA^T) - \frac{2}{7}\bar{\alpha}(L_1^2 \otimes BB^T) \right] \breve{\varphi} \\ & \le \breve{\varphi}^T [L_1 \otimes \mathcal{M}_2]\, \breve{\varphi}, \\ & \le \breve{\varphi}^T [L_1 \otimes (AP + PA^T - \varrho BB^T)]\breve{\varphi} \\ & \le -\theta \breve{\varphi}^T (L_1 \otimes P)\breve{\varphi} = -\theta V_1\end{aligned} \tag{3.71}$$

For the remaining part of (3.69), substitute $\phi = \hat{\phi} + \tilde{\phi}$, one obtains

$$\begin{aligned}& -\frac{12}{7}\phi^T (I_N \otimes \Gamma)\phi + 2\phi^T (I_N \otimes \Gamma)\tilde{\phi} \\ & = -\frac{12}{7}\hat{\phi}^T (I_N \otimes \Gamma)\hat{\phi} - \frac{10}{7}\hat{\phi}^T (I_N \otimes \Gamma)\tilde{\phi} \\ & \quad +\frac{2}{7}\tilde{\phi}^T (I_N \otimes \Gamma)\tilde{\phi}\end{aligned} \tag{3.72}$$

By Young's inequality

$$-\frac{10}{7}\hat{\phi}^T (I_N \otimes \Gamma)\tilde{\phi} \le \frac{5}{7}\hat{\phi}^T (I_N \otimes \Gamma)\hat{\phi} + \frac{5}{7}\tilde{\phi}^T (I_N \otimes \Gamma)\tilde{\phi}$$

Hence

$$-\tfrac{12}{7}\phi^T(I_N\otimes\Gamma)\phi+2\phi^T(I_N\otimes\Gamma)\tilde{\phi}$$
$$\le -\hat{\phi}^T(I_N\otimes\Gamma)\hat{\phi}+\tilde{\phi}^T(I_N\otimes\Gamma)\tilde{\phi}.$$

The latter is conservatively relaxed to the trigger-compatible form

$$-\hat{\phi}^T(I_N\otimes\Gamma)\hat{\phi}+\tilde{\phi}^T(I_N\otimes\Gamma)\tilde{\phi}$$
$$\le -\frac{2}{7}\hat{\phi}^T(I_N\otimes\Gamma)\hat{\phi}+\frac{57}{7}\tilde{\phi}^T(I_N\otimes\Gamma)\tilde{\phi} \quad (3.73)$$

Set

$$r_i = u_{N+1}-\varepsilon_i-d_i$$
$$c_2 = \kappa+\varepsilon_M+d_M$$

The standing bounds imply $\|r_i\|_\infty \le c_2$. Since $\phi=(L_1\otimes I_n)\varphi$ and $QB=-F^T$, then

$$-2\varphi^T(L_1\otimes QB)(\mathbf{1}_N\otimes u_{N+1}-\varepsilon-d)$$
$$=2\sum_{i=1}^{N}(F\phi_i)^T r_i \le 2c_2\|(I_N\otimes F)\phi\|_1 \quad (3.74)$$

Consequently

$$-2\bar{\beta}\|(I_N\otimes F)\phi\|_1-2\varphi^T(L_1\otimes QB)$$
$$\cdot(\mathbf{1}_N\otimes u_{N+1}-\varepsilon-d)$$
$$\le -2(\bar{\beta}-c_2)\|(I_N\otimes F)\phi\|_1\le 0 \quad (3.75)$$

Combining (3.71), (3.73), and (3.75) with (3.68) gives

$$\sum_{j=1}^{3}\dot{V}_j \le -\theta V_1+\sum_{i=1}^{N}q_i^L$$
$$-\hat{\alpha}V_{2\alpha}-\hat{\beta}V_{2\beta}-\hat{r}_1V_{3a}-\hat{r}_2V_{3b} \quad (3.76)$$

where

$$q_i^L=\tfrac{57}{7}\bar{\alpha}\tilde{\phi}_i^T\Gamma\tilde{\phi}_i-\tfrac{2}{7}\bar{\alpha}\hat{\phi}_i^T\Gamma\hat{\phi}_i$$

With $h_i=\eta_i e^{-\gamma t}$, (3.53) can be written as

$$\dot{\eta}_i=-\rho_i\eta_i-(1-\rho_i)q_i^L e^{\gamma t}$$

Thus

$$\dot{V}_4 = -\sum_{i=1}^{N}(\rho_i+\gamma)h_i-\sum_{i=1}^{N}(1-\rho_i)q_i^L \quad (3.77)$$

Between events, $q_i^L\le h_i$, and therefore

$$\sum_{i=1}^{N}q_i^L+\dot{V}_4 = \sum_{i=1}^{N}\rho_i(q_i^L-h_i)$$
$$-\gamma\sum_{i=1}^{N}h_i\le -\gamma V_4 \quad (3.78)$$

It follows that

$$\dot{V} \le -\theta V_1-\hat{\alpha}V_{2\alpha}-\hat{\beta}V_{2\beta}$$
$$-\hat{r}_1V_{3a}-\hat{r}_2V_{3b}-\gamma V_4$$
$$\le -\bar{\theta}V \quad (3.79)$$

where $\bar{\theta}=\min\{\theta,\hat{\alpha},\hat{\beta},\hat{r}_1,\hat{r}_2,\gamma\}$.

Hence

$$V(t)\le V(0)e^{-\bar{\theta}t}$$

Finally

$$V_1 = \varphi^T(L_1\otimes Q)\varphi$$
$$\ge \lambda_{\min}(L_1)\lambda_{\min}(Q)\|\varphi\|^2$$
$$= \frac{\lambda_{\min}(L_1)}{\lambda_{\max}(P)}\|\varphi\|^2=a_2\|\varphi\|^2 \quad (3.80)$$

Therefore

$$\|\varphi(t)\|\le\sqrt{\tfrac{V(0)}{a_2}}e^{-\bar{\theta}t/2}$$

because the ith block of φ is exactly x_i-x_{N+1}, $\|x_i(t)-x_{N+1}(t)\|\to 0$ for every follower i. This proves exact asymptotic leader tracking. □

Corollary 2 *Under Assumptions 1 and 2, the reset convention (3.49), and the trigger (3.52), no triggering sequence of an individual follower can accumulate in finite time.*

Proof Suppose that the events of follower i accumulate at a finite time T. The threshold comparison established after (3.53) gives

$$h_i(t) = \eta_i(t)e^{-\gamma t}\ge \eta_i(0)e^{-(1+\gamma)T}=:h_{i,T}>0$$

for $0\le t<T$.

At a release, $\tilde{\phi}_i(t_k^i)=0$, so

$$q_i^L(t_k^i)=-\tfrac{2}{7}\bar{\alpha}\,\hat{\phi}_i^T(t_k^i)\Gamma\hat{\phi}_i(t_k^i)\le 0$$

thus the post-reset trigger function $g_i^L=q_i^L-h_i$ starts below $-h_{i,T}$. On the finite interval $[0,T)$, Assumption 1 bounds the plant states and the basis signals; the adaptive differential equations have bounded coefficients and bounded forcing on each such interval, so the adaptive variables remain finite there. Consequently, the derivative of g_i^L is essentially bounded between events. The same integration argument as in Theorem 2 gives a strictly positive lower bound on each inter-event interval, contradicting finite-time accumulation. □

Remark 8 (Continuation in the tracking case) The compact-state condition bounds the leader and follower states on every finite interval of existence. The adaptive equations have at most linear growth in the adaptive variables on each such interval, so no adaptive state can blow up in finite time. Together with the positive inter-event lower bound, this rules out both finite escape and Zeno accumulation. Thus, maximal leader–follower solutions are forward complete under Assumption 1.

Remark 9 The functions V_2 and V_3 contain exponentially weighted errors for α_i, $\hat{W}_i$, and $\bar{W}_i$; the leader–follower proof also weights the β_i error. Hence $V(t)\le V(0)e^{-\bar{\theta}t}$ bounds these weighted quantities but

does not, by itself, establish uniform bounds for the corresponding unweighted adaptive variables on $[0,\infty)$. The theorems give the stated coordination-error decay and exclude finite-time event accumulation under their assumptions; they do not prove neural-weight convergence or all-time boundedness of every unweighted adaptive state.

Corollary 3 *For the leaderless design, suppose in addition to Theorem 1 that*

$$\hat{\alpha} = \hat{r}_1 = \hat{r}_2 = \gamma =: r_c$$
$$0 < r_c \le \min\{\theta, 2\lambda_\beta\}$$

then $\bar{\theta} = r_c$, for every i, we have

$$|\alpha_i(t) - \bar{\alpha}| \le \sqrt{k_i V(0)}$$
$$\|\widetilde{W}_i(t)\|_F \le \sqrt{\tau_i V(0)}$$
$$\|\widehat{W}_i(t)\|_F \le \sqrt{\pi_i V(0)}$$
$$0 < \eta_i(t) \le V(0)$$

together with (3.13)*, all adaptive states entering the leaderless controller are uniformly bounded.*

For the leader–follower design, if

$$\hat{\alpha} = \hat{\beta} = \hat{r}_1 = \hat{r}_2 = \gamma =: r_c \qquad 0 < r_c \le \theta$$

then $\bar{\theta} = r_c$ and

$$|\alpha_i(t) - \bar{\alpha}| \le \sqrt{k_i V(0)}$$
$$|\beta_i(t) - \bar{\beta}| \le \sqrt{v_i V(0)}$$
$$\|\widetilde{W}_i(t)\|_F \le \sqrt{\tau_i V(0)}$$
$$\|\widehat{W}_i(t)\|_F \le \sqrt{\pi_i V(0)}$$
$$0 < \eta_i(t) \le V(0)$$

with the common-rate specialization, the unweighted adaptive states remain uniformly bounded. Combining this result with Assumption 1 ensures that the current and held aggregate signals, together with the basis functions, remain bounded. Consequently, the associated control inputs are uniformly bounded.

Proof For example, in the leaderless case

$$\tfrac{(\alpha_i-\bar{\alpha})^2}{k_i} e^{-r_c t} \le V(t) \le V(0) e^{-r_c t}$$

and cancelling the common exponential factor gives the first bound. The two neural-weight bounds and the threshold bound follow in exactly the same way from the corresponding summands of V_3 and V_4. The leader–follower β_i bound follows from its exponentially weighted term in V_2. □

Remark 10 The results derived in this paper provide sufficient conditions for coordination; their necessity is not established. The spectral arguments rely on an undirected and connected follower graph. For leader–follower tracking, the matrix L_1 must also be symmetric positive definite. The associated gain constraints depend on the graph topology and must be verified jointly with the plant LMI, as illustrated by the two parameter sets considered in the numerical examples. The approximation-domain requirement in Assumption 1 deserves particular attention. The Lyapunov analysis alone does not guarantee that the state of an arbitrary nonlinear plant remains within the prescribed NN approximation domain. In practice, this requirement should be verified for the plant under consideration. One possible approach is to identify a forward-invariant operating region and establish a suitable boundary condition, such as the tangent condition introduced above. The uniform boundedness result for the unweighted adaptive states also relies on the common-rate specialization in Corollary 3. No corresponding guarantee is asserted when the exponential rates are chosen independently. Moreover, Condition 1 serves a purpose distinct from the coordination analysis. Excitation observed over a finite simulation interval does not, by itself, verify uniform persistent excitation. Finally, the proposed event-triggering mechanism is formulated under ideal continuous-time monitoring. The finite monitoring grid used in Section 4 provides a numerical approximation to this mechanism. Its implementation and simulation results should not be interpreted as establishing a sampled-data stability theorem.

Proposition 1 *For either controller, write $y_i = F\delta_i$ and $\hat{y}_i = F\hat{\delta}_i$ in the leaderless case, or $y_i = F\phi_i$ and $\hat{y}_i = F\hat{\phi}_i$ in the leader–follower case. Consider, for comparison, a modification that replaces only the current signum signal in the control input by a held signal $\xi_i(t) \in \mathrm{Sgn}(\hat{y}_i(t))$, while the corresponding adaptive law continues to use the current signal $y_i(t)$. On any trajectory for which $\beta_i(t) \ge 0$, the robust-feedback contribution and the cross-term part of the β_i-adaptation contribution to the Lyapunov derivative combine as*

$$\begin{aligned} &-2\beta_i y_i^T \xi_i + 2(\beta_i - b_i)\|y_i\|_1 \\ &= -2b_i\|y_i\|_1 + \Delta_i \end{aligned} \tag{3.81}$$

where $b_i = \beta_i^\circ$ for the leaderless controller and $b_i = \bar{\beta}$ for the leader–follower controller, and

$$\Delta_i := 2\beta_i\big(\|y_i\|_1 - y_i^T\xi_i\big)$$

the mismatch term satisfies

$$0 \le \Delta_i \le 4\beta_i\|y_i - \hat{y}_i\|_1 = 4\beta_i\|F\tilde{\delta}_i\|_1 \tag{3.82}$$

in the leaderless case, with the analogous expression $4\beta_i\|F\tilde{\phi}_i\|_1$ in the leader–follower case.

Proof The cross-term part of the gain-adaptation derivative is $2(\beta_i - b_i)\|y_i\|_1$ for both designs: in the leader–follower case, the exponential factor in the gain-error term cancels the factor $e^{\hat{\beta}t}$ in $\dot{\beta}_i$. Adding

this term to the robust-feedback term $-2\beta_i y_i^T \xi_i$ gives (3.81). In the leaderless design, the target-centred leakage contributes the additional nonpositive term $-2\lambda_\beta(\beta_i - \beta_i^\circ)^2/v_i$ to $\dot{V}$; it is unchanged by the comparison and is not included in Δ_i. Since $\xi_i \in \mathrm{Sgn}(\hat{y}_i)$, each component satisfies $|\xi_{ij}| \le 1$, so $y_i^T \xi_i \le \|y_i\|_1$ and $\Delta_i \ge 0$. Componentwise, the definition of the Filippov sign map gives

$$|y_{ij}| - y_{ij}\xi_{ij} \le 2|y_{ij} - \hat{y}_{ij}|$$

Summing over components and multiplying by $2\beta_i \ge 0$ yields

$$\Delta_i \le 4\beta_i \|y_i - \hat{y}_i\|_1$$

Finally, $y_i - \hat{y}_i = F(\delta_i - \hat{\delta}_i) = F\tilde{\delta}_i$ or $F(\phi_i - \hat{\phi}_i) = F\tilde{\phi}_i$, respectively. □

Remark 11 Proposition 1 concerns an alternative controller and does not change the laws in Theorems 1 and 3. With the current aggregate in the signum map, the mismatch term Δ_i does not appear in the derivative estimate. For leader–follower tracking, the sufficient condition $\bar{\beta} > \kappa + \varepsilon_M + d_M$ makes the robust gain dominate the leader input, approximation residual, and follower disturbance. The lower bound on $\bar{\alpha}$ depends on $\lambda_{\min}(L_1)$. As in the leaderless case, online signals are local, but gain selection uses a graph-level spectral quantity.

Corollary 4 *Under Theorem 3, one has*

$$\|\varphi(t)\| \le \sqrt{\frac{V(0)}{a_2}} e^{-\bar{\theta}t/2} \tag{3.83}$$

for any $r > 0$, a conservative entrance time into $\|\varphi\| \le r$ is

$$T_r = \max\left\{0, \frac{1}{\bar{\theta}} \ln \frac{V(0)}{a_2 r^2}\right\} \tag{3.84}$$

4 Numerical Results

Two ten-agent examples are used to assess the state response and the number of aggregate-buffer updates required by the proposed design. The controller and adaptive laws are implemented as specified in Section 3. No gain freezing, dead zone, prescribed dwell time, input saturation, or boundary-layer approximation is introduced. The closed-loop equations are integrated by the forward Euler method. The nominal integration step is $h_0 = 10^{-3}$ s. At each grid point, the event condition is evaluated before the held aggregate, control input, and adaptive states are advanced. To examine discretization effects, the calculations are repeated with steps of 5×10^{-4}, 2.5×10^{-4}, 1.25×10^{-4}, and 6.25×10^{-5} s. Terminal errors and buffer-refresh counts are compared across the five grids. The finest-grid run is included as a numerical sensitivity check; it is not used to redefine the continuous-time triggering law. This refinement study assesses numerical sensitivity to the integration step. It is not a stability proof for a sampled-data controller. Since event checks are performed only at grid points, the recorded release times approximate those of the continuous-time triggering rule.

For each case, we record the number of aggregate-buffer refreshes, the minimum and mean inter-event intervals, and the peak and root-mean-square coordination errors. Two periodic schemes serve as benchmarks. The first refreshes every agent's held aggregate at each 1 ms grid point; the second selects a period from a finite set of grid-aligned candidates.

Let

$$\begin{aligned}\mathcal{M}_0 &= \{1, 2, 3, 5, 8, 10, 15, 20, 30, 50, 75, 100,\\ &\quad 150, 200, 300, 500, 750, 1000, 1500, 2000,\\ &\quad 3000, 4000, 5000, 7500, 10000\}\\ \mathcal{M}_T &= \{m \in \mathcal{M}_0 : mh_0 \le T\}\end{aligned}$$

The selected periodic interval is the largest tested value of mh_0 that simultaneously matches the event-triggered terminal, peak, and RMS errors to within 10% relative tolerance. The terminal-error condition is $|e_{T,\mathrm{per}} - e_{T,\mathrm{ET}}| \le 0.1 \max\{e_{T,\mathrm{ET}}, \epsilon_{\mathrm{mach}}\}$; analogous conditions are imposed on the peak and RMS errors. Here, all three quantities are computed over the same finite horizon and with the same initial conditions, plant, disturbance, and adaptive laws. This multi-metric criterion avoids selecting a periodic baseline that matches only the terminal value while producing a substantially different transient response. The search is restricted to the finite candidate set; it is not an optimization over all positive periods. All measures are finite-horizon quantities for the prescribed initial conditions and inputs. Refresh counts exclude the common initialization at $t = 0$ and refer to aggregate-buffer updates rather than individual packets.

Two additional ablations are evaluated with the same plant, initial conditions, disturbance realization, integration step, and adaptive linear/robust channels. In the static-threshold baseline, the auxiliary dynamic threshold is replaced by the constant

value $h_i(t) = \eta_i(0)$, while the quadratic trigger signal is retained. In the NN-disabled baseline, the NN compensation term is removed from the input and the associated online weight updates are suspended. These runs are comparative numerical tests only; no stability claim is assigned to either modified baseline. Their purpose is to isolate the finite-horizon effects of threshold adaptation and NN compensation without changing the nominal theorem-level controller.

The implemented controller contains the adaptive states $\hat{W}_i$ and $\bar{W}_i$. An additional finite-memory least-squares (LS) estimate, denoted by $\hat{W}_i^{\mathrm{LS}}$, is computed only for post-processing and is not fed back into the control law. Each example specifies its own state-dependent approximation residual and phase-shifted multisine disturbance. Moving-window Gramians and finite-memory information matrices are evaluated along the simulated trajectories. These quantities describe excitation over the available record only; they do not verify uniform persistent excitation, prove invariance of an arbitrary approximation domain, or establish parameter convergence. The leaderless case emphasizes adaptation of the robust gains toward their prescribed targets, while the leader–follower case examines tracking with sparse leader pinning.

Two sensitivity tests are carried out with the other nominal settings unchanged. First, the disturbance amplitude is scaled while the other nominal settings are fixed. The leaderless case uses $s_d \in \{0.5, 1.0, 1.05\}$, whereas the leader–follower case uses $s_d \in \{0.5, 1.0, 1.1\}$. In the tracking case, the scaling applies only to follower disturbances; the leader's probing signal is left unchanged. These case-dependent upper values preserve the respective sufficient robust-gain inequalities. Second, the initial dynamic threshold is set to $\eta_i(0) = s_\eta \eta_{i,\mathrm{nom}}(0)$, where $s_\eta \in \{0.5, 1.0, 2.0\}$. Only disturbance scales that retain the sufficient robust-gain inequalities are considered. The resulting data compare selected finite-horizon responses and do not imply uniform robustness across the parameter range.

Excitation is evaluated over moving windows using

$$G_i(t; T_{\mathrm{PE}}) = \int_t^{t+T_{\mathrm{PE}}} S_i(x_i(s)) S_i^T(x_i(s))\, ds \qquad (4.1)$$

Only windows that lie entirely within the recorded horizon are included. Thus, $\lambda_{\min}(G_i)$ is a finite-record indicator and not a verification of Condition 1. For the auxiliary LS calculation, introduce

$$\begin{aligned} & H_i(t) \\ &= \int_0^{\min\{t,T_m\}} \frac{S_i(x_i(s)) S_i^T(x_i(s))}{1 + S_i^T(x_i(s)) S_i(x_i(s))}\, ds \\ & b_i(t) \\ &= \int_0^{\min\{t,T_m\}} \frac{S_i(x_i(s)) \hat{f}_i^T(s)}{1 + S_i^T(x_i(s)) S_i(x_i(s))}\, ds \end{aligned} \qquad (4.2)$$

the signal $\hat{f}_i$ is reconstructed from the state trajectory by a one-step backward difference, using the previously applied input and the known disturbance. Once $\lambda_{\min}(H_i)$ exceeds the prescribed rank threshold, the estimate is updated according to

$$\begin{aligned} W_{i,\mathrm{LS}} &= (H_i + \varepsilon_{\mathrm{LS}} I)^{-1} b_i \\ \dot{\hat{W}}_i^{\mathrm{LS}} &= k_W \big(W_{i,\mathrm{LS}} - \hat{W}_i^{\mathrm{LS}}\big) \end{aligned} \qquad (4.3)$$

Data collection is terminated at T_m. The LS variables remain outside the feedback loop, and the nonzero approximation residual may introduce bias into the resulting estimates.

Example 1 Consider the following leaderless network of ten agents. The communication graph $\mathcal{G} = (\mathcal{V}, \mathcal{E})$ is undirected and connected, with $\mathcal{V} = \{1, \ldots, 10\}$ and

$$\begin{aligned} \mathcal{E} = \{\ & (1,2), (1,3), (1,8), (1,10), 2,3), (2,4), \\ & ((3,4), (3,6), (4,5), (4,9), (5,6), (5,7), \\ & (6,7), (7,8), (7,10), (8,9), (9,10)\} \end{aligned} \qquad (4.4)$$

thus, the graph contains 17 undirected edges; its degree sequence is $(4, 3, 4, 4, 3, 3, 4, 3, 3, 3)$.

The same follower-interaction graph is used in the leader–follower example below

$$\dot{x}_i(t) = A x_i(t) + B\big[u_i(t) + f_i(x_i(t)) + d_i(t)\big] \qquad (4.5)$$

for $i = 1, \ldots, 10$. where

$$A = \begin{bmatrix} 0 & 1 \\ -1 & -2 \end{bmatrix} \qquad B = \begin{bmatrix} 0 \\ 1 \end{bmatrix}$$

The matrix A is Hurwitz. The certificate is specified by

$$\begin{aligned} P^{-1} &= \begin{bmatrix} 7.9996 & 5.1619 \\ 5.1619 & 5.0200 \end{bmatrix} \\ P &= \begin{bmatrix} 0.3715 & -0.3820 \\ -0.3820 & 0.5920 \end{bmatrix} \\ F &= -B^T P^{-1} = \begin{bmatrix} -5.1619 & -5.0200 \end{bmatrix} \\ \Gamma &= F^T F \end{aligned}$$

The certificate satisfies $\lambda_{\max}(AP + PA^T - 2BB^T + P) = -0.2606 < 0$.

The first example considers ten constrained-guideway mobile units represented by a longitudinal second-order model. The coordinate q_i denotes the longitudinal displacement and v_i the velocity of robot i. A low-level velocity servo is represented by a virtual acceleration input, so this example is a reduced-order guideway-coordination model rather than a full planar robot kinematic model. The nominal guideway dynamics include linear restoring and viscous-damping effects, while uncertain terrain forces and nonlinear rolling resistance are included in the matched term. With $x_i = [q_i, v_i]^T$, the plant equations are

$$\dot{q}_i = v_i \tag{4.6}$$
$$\dot{v}_i = -q_i - 2v_i + u_i + f_i(x_i) + d_i(t) \tag{4.7}$$

where $-q_i$ represents the nominal guideway restoring effect and $-2v_i$ the nominal viscous resistance. The matched uncertainty f_i captures unmodelled terrain forces and velocity-dependent rolling resistance. The neural basis and residual are specified as

$$\begin{aligned} S_i(x_i) &= \begin{bmatrix}\tanh x_{i1} & \tanh x_{i2}\end{bmatrix}^T \\ f_i(x_i) &= W_i^{\star T} S_i(x_i) + \varepsilon_i(x_i) \end{aligned} \tag{4.8}$$

where

$$\begin{aligned} W_i^\star &= \begin{bmatrix}0.4500 \\ -0.3500\end{bmatrix} + (i-1)\begin{bmatrix}0.0150 \\ 0.0100\end{bmatrix} \\ \varepsilon_i(x_i) &= 0.0050\sin(x_{i1} + 0.7000x_{i2} + 0.1700i) \\ &\quad -\kappa_i \tanh^3(x_{i1}) - c_i \tanh(x_{i2})|\tanh(x_{i2})| \end{aligned}$$

where $\kappa_i = 0.0080 + 0.0003(i-1)$ and $c_i = 0.0080 + 0.0003(i-1)$. The term $-\kappa_i \tanh^3(q_i)$ represents a bounded nonlinear terrain-restoring force, whereas $-c_i \tanh(v_i)|\tanh(v_i)|$ models nonlinear rolling resistance. Since $|\tanh(s)| \le 1$, the complete residual satisfies $|\varepsilon_i(x_i)| \le \varepsilon_M = 0.0264$ for every $x_i \in \mathbb{R}^2$. The phase-shifted disturbance is

$$d_i(t) = \sum_{k=1}^{4} a_k \sin\big(\omega_k t + \phi_k + 0.3700(i-1)\big) \tag{4.9}$$

with $(a_k) = (0.1000, 0.0700, 0.0500, 0.0300)$, $(\omega_k) = (1.2000, 2.7000, 4.5000, 6.8000)$, and $(\phi_k) = (0, 0.4000, 0.8000, 1.2000)$. Hence $|d_i(t)| \le d_M = 0.2500$.

The initial conditions are

$$\begin{aligned} x_1(0) &= \begin{bmatrix}0.1200 \\ -0.0800\end{bmatrix} & x_2(0) &= \begin{bmatrix}-0.1000 \\ 0.1000\end{bmatrix} \\ x_3(0) &= \begin{bmatrix}0.0800 \\ -0.0600\end{bmatrix} & x_4(0) &= \begin{bmatrix}-0.0600 \\ 0.0700\end{bmatrix} \\ x_5(0) &= \begin{bmatrix}0.1400 \\ -0.1100\end{bmatrix} & x_6(0) &= \begin{bmatrix}-0.1200 \\ 0.0900\end{bmatrix} \\ x_7(0) &= \begin{bmatrix}0.0500 \\ -0.0400\end{bmatrix} & x_8(0) &= \begin{bmatrix}0.0400 \\ 0.0500\end{bmatrix} \\ x_9(0) &= \begin{bmatrix}0.0900 \\ -0.0900\end{bmatrix} & x_{10}(0) &= \begin{bmatrix}-0.0700 \\ 0.0600\end{bmatrix} \end{aligned}$$

and

$$\hat{W}_i(0) = \bar{W}_i(0) = \begin{bmatrix}0.1000 + 0.0200(i-1) \\ -0.0800 + 0.0100(i-1)\end{bmatrix}$$

For $t \in [0, 5]$ s, choose

$$\begin{aligned} \varrho &= 2 \quad \theta = 1 \quad k_i = v_i = 0.0100 \\ \tau_i &= 200 \quad \sigma_i = \pi_i = 0.0100 \\ \hat{r}_1 &= \hat{r}_2 = 0.0010 \quad \hat{\alpha} = 0.0010 \\ \bar{\alpha} &= 3 \quad \lambda_\beta = 2 \quad \gamma = 0.0010 \\ \rho_i &= 0.9500 \quad \alpha_i(0) = 0.5000 \\ \eta_i(0) &= 2.2000 \quad \beta_i(0) = 0.0500 + 0.0100(i-1) \end{aligned}$$

The chosen rates meet the common-rate requirement in Corollary 3 with $r_c = 0.0010$. Accordingly, the theorem provides uniform bounds on the unweighted adaptive states.

The target values for the robust gains are set to

$$\beta_i^\circ = 0.3000 + 0.0200(i-1) \tag{4.10}$$

The follower graph is the same as that used in Example 2. Its algebraic connectivity is $\lambda_2(L) = 1.5199$, and the gain constraints are satisfied

$$\bar{\alpha} = 3 > \tfrac{2\varrho}{\lambda_2(L)} = 2.6318$$
$$\min_i\{\beta_i^\circ\} = 0.3000 > \varepsilon_M + d_M = 0.2764$$

The computed margins for the graph-gain inequality, robust-gain bound, and plant LMI are 0.3682, 0.0236, and 0.2606, respectively. Each is positive, confirming feasibility for this parameter set; the theoretical results still rely on the stated assumptions.

The nominal run lasts 5 s and uses a 1 ms monitoring grid. Its terminal disagreement is measured by $\max_i \|x_i(T) - \bar{x}(T)\|$. Figs. 2 and 3 collect the displacement and velocity responses, adaptive gains, aggregate-buffer release instants, representative nonlinear force characteristics, and the two components of the online NN weights $\hat{W}_i(t)$. Nonlinear terrain forces and rolling resistance act throughout the run, together with agent-dependent external disturbances. The coordination error therefore reflects the combined influence of nonlinear mechanical uncertainty and time-varying disturbances. The evolution of β_i shows how the gains move relative to their prescribed targets, but a finite simulation cannot establish the asymptotic result in Theorem 1. In addition to the nominal run, simulations use grid steps of 0.5, 0.25, and 0.125 ms. Grid-refinement and sensitivity data are exported by the accompanying source programs and should be inserted into the final numerical tables only after the updated simulations have been rerun.

The plotted $\hat{W}_i(t)$ trajectories are the online adaptive weights entering the feedback input. Their evolution is shown alongside the nominal approximation

coefficients $W_i^\star$ for reference; the comparison is descriptive and does not assert parameter convergence. The finite-memory least-squares and moving-window excitation outputs are retained as reproducibility diagnostics in the source files; they are not used by the feedback law and are not needed to interpret the main nonlinear coordination results. For the LS diagnostic, we use $T_{\mathrm{PE}} = 0.5000$, $\mu_{\mathrm{PE}} = 10^{-8}$, $T_m = 1.2000$, $k_W = 8$, a rank threshold of 10^{-5}, and $\varepsilon_{\mathrm{LS}} = 10^{-8}$. The minimum eigenvalue of the moving-window Gramian is evaluated over windows contained in $[0, 5]$ s. An agent passes this finite-window test only when the minimum is no smaller than μ_{PE}. The LS calculation uses a noise-free backward-difference reconstruction and stops collecting data at T_m. Since the approximation residual is nonzero, exact recovery of $W_i^\star$ is not generally expected. These finite-record diagnostics do not prove uniform excitation or parameter convergence.

Example 2 The second example considers ten nonlinearly coupled second-order oscillators in a leader–follower configuration under external disturbances. Each oscillator has a displacement-like state q_i and a velocity-like state v_i. The followers use the same connected undirected 10-node, 17-edge interaction graph specified in Example 1. Direct leader information is supplied to followers $1, 3, 5, 7, 9$, each with pinning weight 10; the remaining followers receive leader information through the network. The plant is

$$\dot{x}_i(t) = Ax_i(t) + B\big[u_i(t) + f_i(x_i(t)) + d_i(t)\big] \quad (4.11)$$

Writing $x_i = [q_i, v_i]^T$, the nominal oscillator equations are

$$\begin{aligned} \dot{q}_i &= v_i \\ \dot{v}_i &= -q_i - 2v_i + u_i + f_i(x_i) + d_i(t) \end{aligned} \quad (4.12)$$

here f_i includes nonlinear stiffness and amplitude-dependent damping, and $d_i(t)$ is an agent-dependent external disturbance. where

$$A = \begin{bmatrix} 0 & 1 \\ -1 & -2 \end{bmatrix} \quad B = \begin{bmatrix} 0 \\ 1 \end{bmatrix} \quad P = \begin{bmatrix} 0.3715 & -0.3820 \\ -0.3820 & 0.5920 \end{bmatrix}$$

$$F = -B^T P^{-1} = \begin{bmatrix} -5.1619 & -5.0200 \end{bmatrix}$$

The plant certificate satisfies $\lambda_{\max}(AP + PA^T - 2BB^T + P) = -0.2606$. Direct access to the leader is provided to followers $1, 3, 5, 7, 9$, each with pinning weight 10:

$$\bar{a} = 10\begin{bmatrix} 1 & 0 & 1 & 0 & 1 & 0 & 1 & 0 & 1 & 0 \end{bmatrix}^T \quad \lambda_{\min}(L_1) = 1.9558$$

The matched nonlinear term is chosen as

$$\begin{aligned} S_i(x_i) &= \begin{bmatrix} \tanh x_{i1} & \tanh x_{i2} \end{bmatrix}^T \\ f_i(x_i) &= W_i^{\star T} S_i(x_i) + \varepsilon_i(x_i) \end{aligned} \quad (4.13)$$

where

$$W_i^\star = \begin{bmatrix} 0.5500 \\ -0.4500 \end{bmatrix} + (i-1)\begin{bmatrix} 0.0150 \\ 0.0100 \end{bmatrix}$$

$$\begin{aligned} \varepsilon_i(x_i) = {} & 0.0050 \sin(x_{i1} + 0.6000 x_{i2} + 0.1300 i) \\ & - \bar{\kappa}_i \tanh^3(x_{i1}) - \bar{c}_i \tanh(x_{i2}) |\tanh(x_{i2})| \end{aligned}$$

where $\bar{\kappa}_i = 0.0100 + 0.0002(i-1)$ and $\bar{c}_i = 0.0120 + 0.0002(i-1)$. These terms describe nonlinear stiffness and amplitude-dependent damping. Since $|\tanh(s)| \le 1$, the residual satisfies $|\varepsilon_i(x_i)| \le \varepsilon_M = 0.0340$ for every $x_i \in \mathbb{R}^2$. The leader input is $u_L(t) = -1 + d_L(t)$, with

$$d_L(t) = \sum_{k=1}^{5} c_k \sin(\omega_k t + \psi_k) \quad (4.14)$$

The coefficients are given as

$$\begin{aligned} (c_k) &= (0.1500, 0.1000, 0.0700, 0.0500, 0.0350) \\ (\omega_k) &= (0.8000, 1.9000, 3.3000, 5.1000, 7.4000) \\ (\psi_k) &= (0, 0.4000, 0.8000, 1.1000, 1.5000) \end{aligned}$$

it follows that $\|u_L(t)\|_\infty \le \kappa = 1.4050$. The follower disturbances use the same amplitudes and frequencies, with phase shifts of $0.3100i$. Hence $|d_i(t)| \le d_M = 0.4050$, and the follower disturbances do not cancel the leader's multisine component exactly.

The initial follower states are

$$\begin{aligned} x_1(0) &= \begin{bmatrix} -0.3000 \\ 0.3500 \end{bmatrix} \quad x_2(0) = \begin{bmatrix} 0.2500 \\ -0.2000 \end{bmatrix} \\ x_3(0) &= \begin{bmatrix} -0.2000 \\ 0.3000 \end{bmatrix} \quad x_4(0) = \begin{bmatrix} 0.3500 \\ -0.4000 \end{bmatrix} \\ x_5(0) &= \begin{bmatrix} -0.4000 \\ 0.2500 \end{bmatrix} \quad x_6(0) = \begin{bmatrix} 0.1500 \\ -0.1500 \end{bmatrix} \\ x_7(0) &= \begin{bmatrix} -0.2500 \\ -0.0400 \end{bmatrix} \quad x_8(0) = \begin{bmatrix} 0.0400 \\ 0.2000 \end{bmatrix} \\ x_9(0) &= \begin{bmatrix} 0.3000 \\ -0.3000 \end{bmatrix} \quad x_{10}(0) = \begin{bmatrix} -0.1500 \\ 0.1000 \end{bmatrix} \end{aligned}$$

The leader starts from $x_L(0) = \begin{bmatrix} 0.1000 & -0.0500 \end{bmatrix}^T$, and the NN-weight variables satisfy

$$\hat{W}_i(0) = \bar{W}_i(0) = \begin{bmatrix} 0.1200 + 0.0150(i-1) \\ -0.1000 + 0.0100(i-1) \end{bmatrix} \quad (4.15)$$

For the 10 s simulation, the controller and adaptation parameters are set to

$$\begin{aligned} &\varrho = 2 \quad \theta = 1 \quad k_i = v_i = 0.0100 \\ &\tau_i = 200 \quad \sigma_i = \pi_i = 0.0100 \\ &\hat{r}_1 = \hat{r}_2 = 0.0010 \\ &\hat{\alpha} = \hat{\beta} = 0.0010 \quad \bar{\alpha} = 4 \\ &\bar{\beta} = 2 \quad \gamma = 0.0010 \quad \rho_i = 0.9500 \\ &\alpha_i(0) = \beta_i(0) = \eta_i(0) = 0.0100 \end{aligned}$$

The rates satisfy the common-rate condition in Corollary 3 with $r_c = 0.0010$. The gain inequalities are satisfied as well:

$$\bar{\alpha} = 4 > \frac{7\varrho}{2\lambda_{\min}(L_1)} \approx 3.5792$$

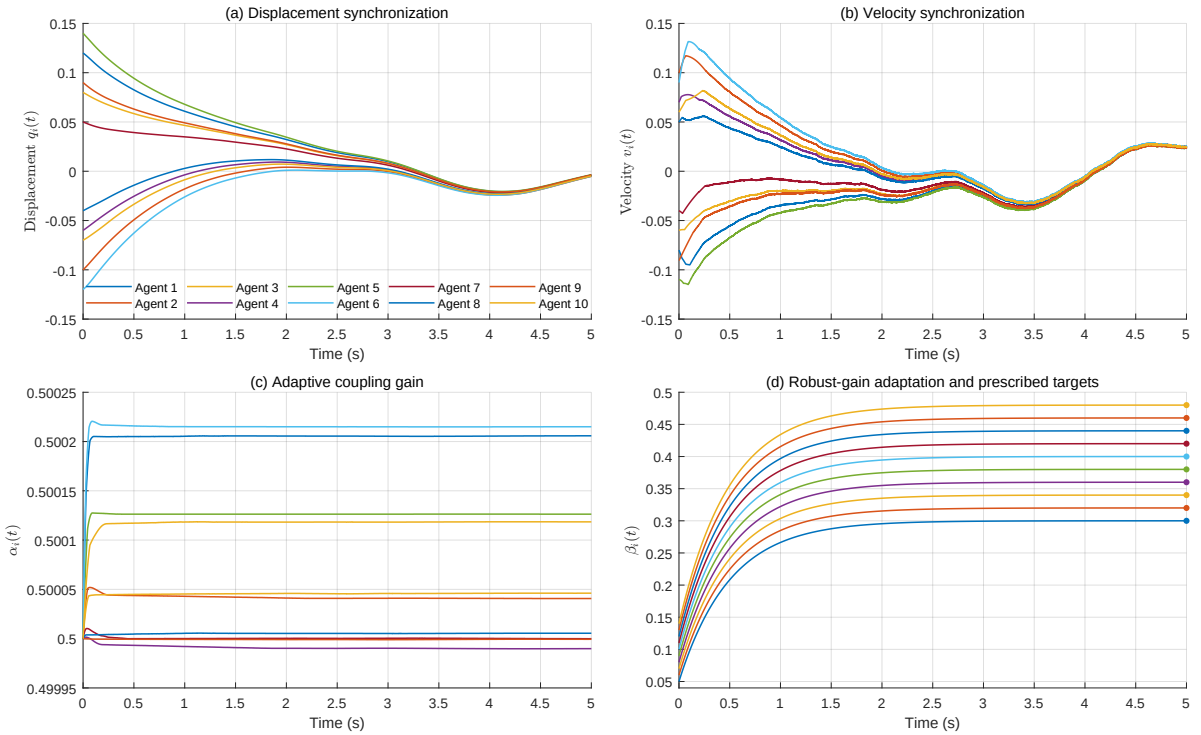


Fig. 2 Leaderless coordination in Example 1: (a) displacement synchronization, (b) velocity synchronization, (c) adaptive coupling gain, and (d) robust-gain adaptation with prescribed targets.

$$\bar{\beta} = 2 > \kappa + \varepsilon_M + d_M = 1.8440$$

For this parameter set, the margins of the graph-gain inequality, robust-gain bound, and plant LMI are 0.4208, 0.1560, and 0.2606, respectively. All are positive. This confirms feasibility of the selected numerical values, while the theorem continues to depend on its stated assumptions.

The nominal tracking run lasts 10 s with a 1 ms grid, and the reported terminal error is $\max_i \|x_i(T) - x_L(T)\|$. The principal responses and control-related quantities are summarized in Figs. 4 and 5, including leader–follower displacement and velocity tracking, adaptive gains, release instants, representative nonlinear force characteristics, and both components of the online NN weights $\hat{W}_i(t)$. Nonlinear stiffness, nonlinear damping, and phase-shifted external disturbances are retained in every run. Both the approximation residual and the phase-shifted follower disturbances are retained throughout the run. Theorem 3 establishes asymptotic tracking under its assumptions. The common-rate condition also bounds the unweighted adaptive states, but it does not guarantee convergence of α_i, β_i, or the NN weights. The same tests are repeated at finer grid resolutions and under the prescribed disturbance-amplitude and initial-threshold variations.

The plotted $\hat{W}_i(t)$ curves are the online weights used by the controller; the nominal coefficients $W_i^\star$ are included only as visual references. Their finite-horizon trajectories do not imply convergence to the nominal coefficients. The finite-memory least-squares and moving-window excitation outputs are retained as reproducibility diagnostics in the source files; they do not enter the control law. For the LS diagnostic, the settings are $T_{\mathrm{PE}} = 1$, $\mu_{\mathrm{PE}} = 10^{-6}$, $T_m = 2.5000$, $k_W = 4$, a rank threshold of 10^{-4}, and $\varepsilon_{\mathrm{LS}} = 10^{-8}$. Only windows fully contained in $[0, 10]$ s are considered. An agent passes the finite-window test if the minimum Gramian eigenvalue is at least μ_{PE}. The LS estimate is reconstructed by the noise-free backward-difference procedure and is not used for feedback. The nonzero residual may bias this estimate; therefore, the diagnostic does not demonstrate uniform excitation or identifiability over an unbounded time horizon.

Both examples use the same Hurwitz matrix $A = \begin{bmatrix} 0 & 1 \\ -1 & -2 \end{bmatrix}$, whose eigenvalues are both equal to -1. The hyperbolic-tangent basis functions, approximation residuals, and exogenous inputs are globally bounded, and the selected adaptation rates meet the common-rate condition used in the adaptive-state bound. In the leaderless case, the disagreement estimate bounds relative

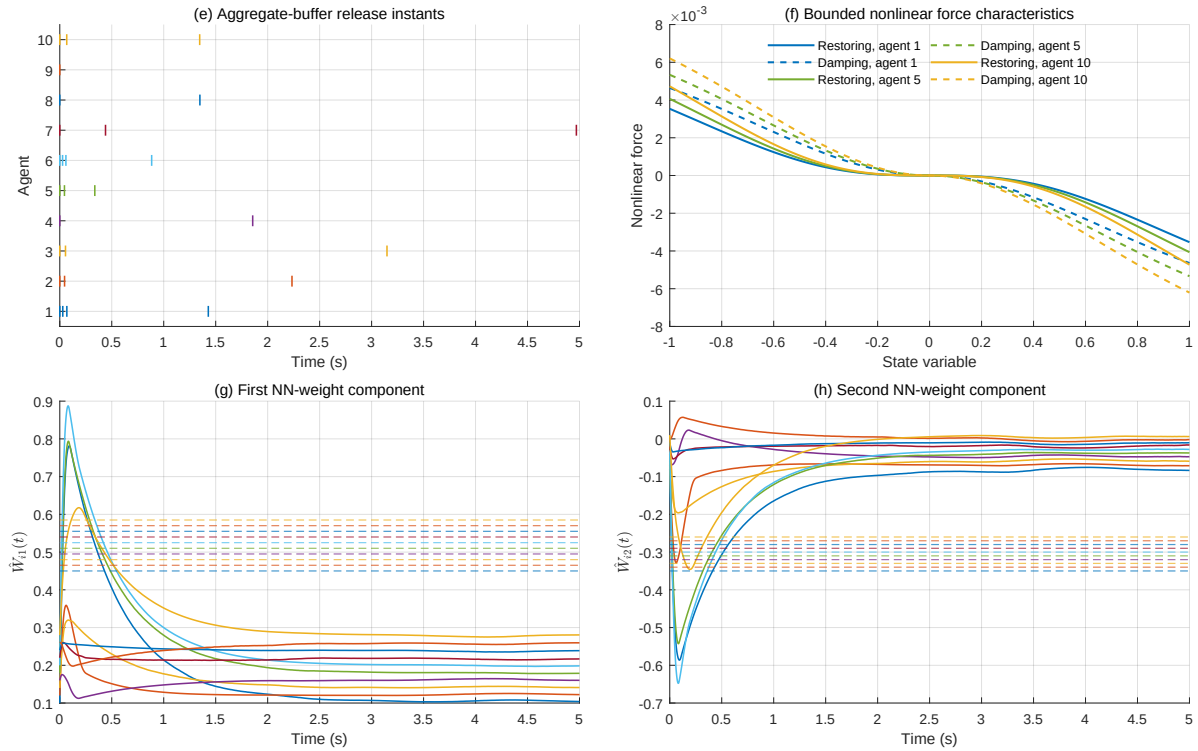


Fig. 3 Additional results for Example 1: (e) aggregate-buffer release instants, (f) bounded nonlinear force characteristics, (g) first component of the online NN weights, and (h) second component of the online NN weights. Solid curves denote $\hat{W}_{ij}(t)$; dashed curves indicate the nominal coefficients $W^{\star}_{ij}$.

states, while the network average evolves according to stable linear dynamics driven by bounded coupling, residual, and disturbance terms. In the tracking case, the reference dynamics are stable and the tracking-error estimate bounds each follower's deviation from the leader. These properties, together with the adaptive-state bounds, support forward completeness and boundedness for the specific models simulated here. In particular, the nonlinear restoring and damping terms are globally bounded because they are composed of bounded hyperbolic-tangent functions; the sinusoidal residuals and external multisine disturbances are bounded as well. The simulations therefore provide model-specific boundedness evidence, not a general invariance proof for an arbitrary compact NN approximation set. The solution-domain assumption remains part of the general theorems.

The examples are reduced-order test cases for networked motion-control systems. Example 1 can represent servo axes or mobile units whose position- and rate-like states must synchronize in the presence of matched nonlinear load terms and bounded periodic disturbances. Example 2 uses a second-order spring–damper oscillator and a dynamically evolving leader reference. Only followers $1, 3, 5, 7, 9$ receive the leader signal directly; the others track through inter-agent coupling. This setup illustrates coordinated motion modules with sparse access to a central reference. It is not identified from a particular commercial platform. The phase-shifted multisine signals are prescribed test inputs rather than field measurements.

In a physical system, an agent could obtain its current aggregate from relative encoder measurements or from range/vision sensing between mobile units. The resulting signal would be supplied to the robust feedback, adaptive laws, and trigger; at a release, it would also be copied to the held buffer used by the linear coupling. In the simulations, each aggregate is computed directly from the states of the graph neighbors. Packet routing, contention, retransmissions, and sensor-bus traffic are not modeled. Thus, the reported counts measure aggregate-buffer refreshes only; they are not counts of network packets or direct estimates of bandwidth, energy use, or computational cost. If

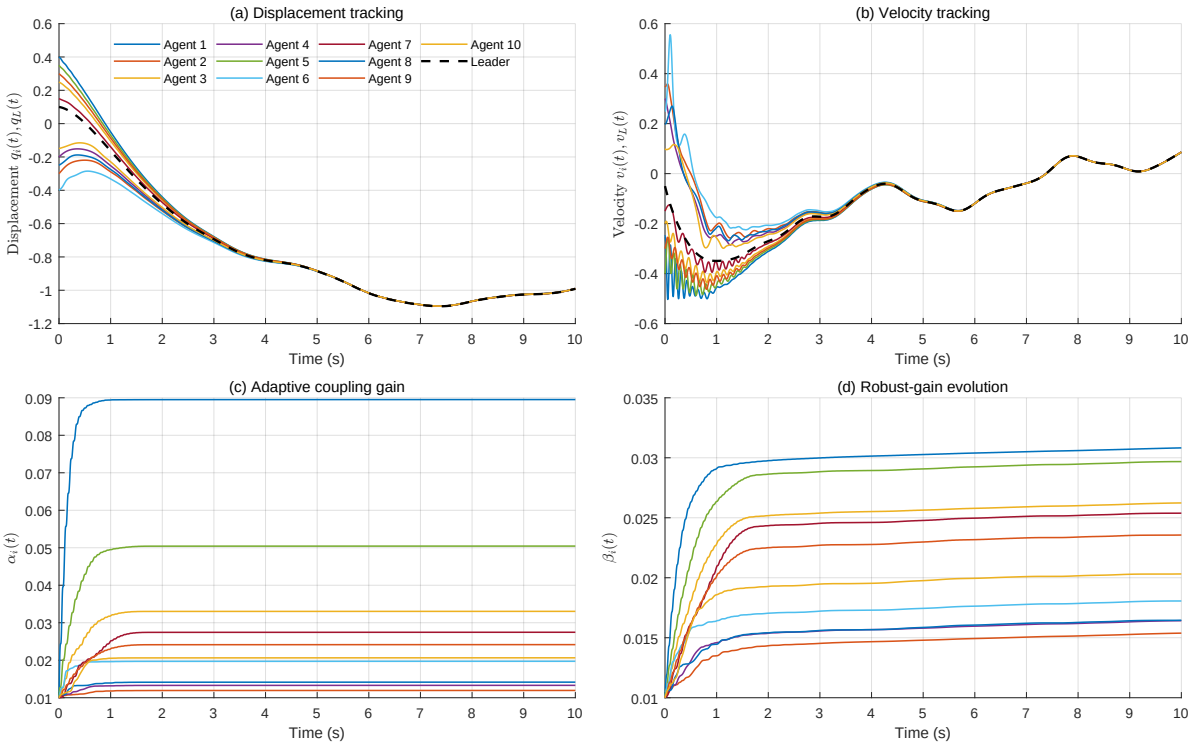


Fig. 4 Leader–follower tracking in Example 2: (a) follower and leader displacement responses, (b) follower and leader velocity responses, (c) adaptive coupling gain, and (d) robust-gain evolution.

aggregates were reconstructed from asynchronous broadcasts, the associated measurement errors and jump dynamics would need to be included in the model and analysis. Actuator saturation, measurement noise, communication delays, and packet losses are also outside the present simulations, so no claim of deployment-level validation is made.

5 Conclusions

An adaptive event-triggered strategy has been developed for consensus and tracking in uncertain nonlinear multi-agent systems. Its key feature is the separation of information channels: the linear coupling uses an aggregate that is refreshed at event times and held between updates, whereas the robust feedback and adaptation laws rely on the current local aggregate. This arrangement preserves the terms needed for the Lyapunov cancellations and allows the effect of the held-signal error to be treated through the dynamic triggering condition. Under the stated plant, graph, gain, and solution-domain assumptions, the analysis establishes complete leaderless consensus, asymptotic leader–follower tracking, exponential error bounds, and the absence of finite-time accumulation of event times. Finite-record excitation and auxiliary least-squares diagnostics are retained as supporting numerical information, rather than as evidence of persistent excitation or ideal weight convergence. The controller still requires current local relative-state information, and the theoretical guarantees rely on the compact approximation-domain condition; forward completeness follows from the finite-time continuation and non-Zeno arguments. Further work will consider actuator constraints, measurement noise, communication delays, packet loss, reconstruction from asynchronous neighbor-only data, and experimental or hardware-in-the-loop validation.

Statements and Declarations

Funding. This work was supported in part by the National Natural Science Foundation of China under Grant Nos. 11301226 and 61572014.

Competing Interests. The authors have no relevant financial or non-financial interests to disclose.

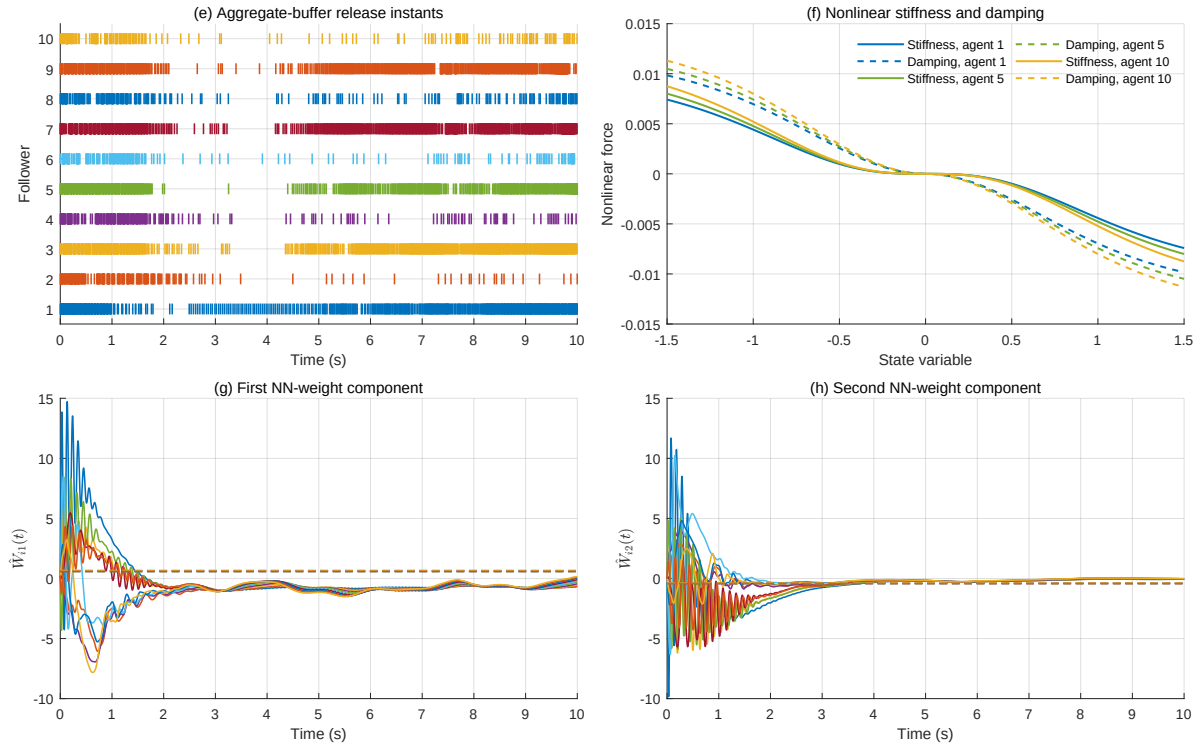


Fig. 5 Additional results for Example 2: (e) aggregate-buffer release instants, (f) nonlinear stiffness and damping characteristics, (g) first component of the online NN weights, and (h) second component of the online NN weights. Solid curves denote $\hat{W}_{ij}(t)$; dashed curves indicate the nominal coefficients $W_{ij}^{\star}$, which are reference values rather than guaranteed asymptotic estimates.

Table 1 Nominal finite-horizon performance and aggregate-buffer update statistics.

Case	e_T	e_{pk}	e_{rms}	$\|u\|_{\mathrm{pk}}$	N_{ET}	$N_{1\mathrm{ms}}$	Reduct.	Mean IET
Leaderless	0.0012	0.1725	0.0412	0.6476	18	50000	99.96%	1.1103
Leader–follower	0.0015	0.8160	0.0963	8.7677	7200	100000	92.80%	0.0225

e_T is the terminal consensus/tracking error; e_{pk} and e_{rms} are the peak and root-mean-square errors; $\|u\|_{\mathrm{pk}}$ is the peak control magnitude; N_{ET} counts aggregate-buffer releases; $N_{1\mathrm{ms}}$ is the number of post-initialization refreshes in the 1-ms periodic reference; IET denotes inter-event time. The reduction is relative to the 1-ms reference and does not represent packet-level traffic.

Data Availability. The numerical data generated and analyzed during the current study, together with the source codes used to produce the reported simulations, are available from the corresponding author on reasonable request.

References

[1] Das A, Lewis F L. Distributed adaptive control for synchronization of unknown nonlinear networked systems. Automatica, 2010, 46(12): 2014-2021.

[2] Das A, Lewis F L. Cooperative adaptive control for synchronization of second-order systems with unknown nonlinearities. International Journal of Robust and Nonlinear Control, 2011, 21(13): 1509-1524.

[3] Zhang H, Lewis F L. Adaptive cooperative tracking control of higher-order nonlinear systems with unknown dynamics. Automatica, 2012, 48(7): 1432-1439.

[4] Peng Z, Wang D, Zhang H, Sun G. Distributed neural network control for adaptive synchronization of uncertain dynamical multiagent systems. IEEE Transactions on Neural Networks and Learning Systems, 2014, 25(8): 1508-1519.

[5] Chen C L P, Wen G X, Liu Y J, et al. Adaptive consensus control for a class of nonlinear multiagent time-delay systems using neural networks. IEEE Transactions on Neural Networks and Learning Systems, 2014, 25(6): 1217-1226.

Table 2 Integration-grid refinement and terminal-error-matched periodic benchmarks.

Case	Grid step (ms)	Terminal error	Aggregate-buffer releases	Relative change
Leaderless	1.000	0.0012	18	–
	0.500	0.0010	17	16.53%
	0.250	0.0012	17	14.14%
	0.125	0.0011	17	5.56%
	0.0625	0.0011	17	2.13%
Leader–follower	1.000	0.0015	7200	–
	0.500	0.0014	4255	0.46%
	0.250	0.0014	3375	0.09%
	0.125	0.0014	3329	0.02%
	0.0625	0.0014	3349	0.01%

The relative change is computed against the immediately preceding coarser-grid terminal error. The event-triggered release times are grid approximations to the continuous-time rule. The finest grid is a numerical refinement check only. The periodic benchmark is retained only when terminal, peak, and RMS errors all satisfy the 10% matching tolerance. For this multi-metric matched periodic benchmark, the selected periods are 1.5000 s and 10.0000 s, with terminal errors 0.0013and 0.0014, peak errors 0.1780and 0.8183, RMS errors 0.0413and 0.0968, and refresh counts 30and 10, respectively; the corresponding reductions are 40.00%and -71900.00%. The periodic search is restricted to the finite candidate set described in the text.

Table 3 Finite-horizon sensitivity to disturbance amplitude and initial dynamic threshold.

Case	Variation	Scale	Terminal error	RMS error	Releases
Leaderless	Disturbance	0.50	0.0012	0.0412	17
	Disturbance	1.05	0.0012	0.0412	17
	Initial threshold	0.50	0.0011	0.0412	51
	Initial threshold	2.00	0.0013	0.0412	14
Leader–follower	Disturbance	0.50	0.0012	0.0963	6837
	Disturbance	1.10	0.0015	0.0963	7033
	Initial threshold	0.50	0.0014	0.0963	7127
	Initial threshold	2.00	0.0015	0.0963	6841

The disturbance scale multiplies follower/agent-side disturbances; in the leader–follower example, the leader probing signal is unchanged. The threshold scale multiplies the nominal initial value $\eta_i(0)$. The disturbance upper scales differ between the two cases to retain the corresponding robust-gain inequalities. All entries are finite-horizon results.

Table 4 Controlled ablation results for the static-threshold and NN-disabled baselines.

Case	Controller variant	Terminal error	Peak error	RMS error	Releases
Leaderless	Proposed DETM–NN	0.0012	0.1725	0.0412	18
	Static threshold	0.0013	0.1726	0.0412	8
	NN disabled	0.0014	0.1704	0.0412	18
Leader–follower	Proposed DETM–NN	0.0015	0.8160	0.0963	7200
	Static threshold	0.0015	0.8160	0.0963	3915
	NN disabled	0.1239	0.5876	0.1779	794

All entries are generated by the accompanying scripts. The static-threshold and NN-disabled variants are ablations, not theorem-certified controllers. The release count refers to aggregate-buffer refreshes only.

[6] Wen G X, Chen C L P, Liu Y J, et al. Neural-network-based adaptive leader-following consensus control for second-order nonlinear multi-agent systems. IET Control Theory and Applications, 2015, 9(13): 1927-1934.

[7] Sun J, Geng Z. Adaptive consensus tracking for linear multi-agent systems with heterogeneous unknown nonlinear dynamics. International Journal of Robust and Nonlinear Control, 2016, 26(1): 154-173.

[8] Sun J, Geng Z, Lv Y. Adaptive output feedback consensus tracking for heterogeneous multi-agent systems with unknown dynamics under directed graphs. Systems and Control Letters, 2016, 87: 16-22.

[9] Wen G, Wang P, Huang T, et al. Robust neuro-adaptive containment of multileader multiagent systems with uncertain dynamics. IEEE Transactions on Systems, Man, and Cybernetics: Systems, 2019, 49(2): 406-417.

[10] Sun N, Zhang T. Observer-based adaptive memory event-triggered consensus tracking control for high-speed train under DoS attacks. Nonlinear Dynamics, 2024, 112: 18377–18395.

[11] El-Ferik S, Hashim H A, Lewis F L. Neuro-adaptive distributed control with prescribed performance for the synchronization of unknown nonlinear networked systems. IEEE Transactions on Systems, Man, and Cybernetics: Systems, 2018, 48(12): 2135-2144.

[12] Li H, Zhang J, Jing L, et al. Neural-network-based adaptive quasi-consensus of nonlinear multi-agent systems with communication constraints and switching topologies. Nonlinear Analysis: Hybrid Systems, 2020, 35: 100833.

[13] Yue D, Cao J, Li Q, Liu Q. Neural-network-based fully distributed adaptive consensus for a class of uncertain multiagent systems. IEEE Transactions on Neural Networks and Learning Systems, 2021, 32(7): 2965-2977.

[14] He W, Xu B, Han Q L, et al. Adaptive consensus control of linear multiagent systems with dynamic event-triggered strategies. IEEE Transactions on Cybernetics, 2019, 50(7): 2996-3008.

[15] Li S, Zou W, Xiang Z. Neural-network-based consensus of multiple Euler-Lagrange systems with an event-triggered mechanism. Journal of the Franklin Institute, 2021, 358(16): 8625-8638.

[16] Liu Z, Liang H, Xue H. Event-triggered funnel control for network systems with unknown dynamic leader based on BP neural networks. Neurocomputing, 2022, 502: 15-26.

[17] Li X, Long L. Distributed dynamic event-triggered adaptive neural resilient control for switched multiagent systems against attacks. Nonlinear Dynamics, 2025, 113: 21583–21600.

[18] Wang Z, Zhu Y, Xue H, et al. Neural networks-based adaptive event-triggered consensus control for a class of multi-agent systems with communication faults. Neurocomputing, 2022, 470: 99-108.

[19] Xiao Y, Che W W. Neural-networks-based event-triggered consensus tracking control for nonlinear MASs with DoS attacks. Neurocomputing, 2022, 501: 451-462.

[20] Xie X, Liu Y, Li Q. Neural network-based adaptive event-triggered control for cyber–physical systems under resource constraints and hybrid cyberattacks. Automatica, 2023, 152: 110977.

[21] Li H, Cao J. Event-triggered group consensus for one-sided Lipschitz multi-agent systems with input saturation. Communications in Nonlinear Science and Numerical Simulation, 2023, 121: 107234.

[22] Li H, Cao J. Observer-based output feedback event-triggered bounded consensus of multi-agent systems under DoS attacks. Communications in Nonlinear Science and Numerical Simulation, 2024, 131: 107843.

[23] Wang J Q, Wang Y. Fully distributed dynamic event-triggered control for bipartite consensus of input constrained multiagent systems. Communications in Nonlinear Science and Numerical Simulation, 2026, 153: 109513.

[24] Cui H, Zhao G, Hua C, Cui R, Ding W. Adaptive double-event triggering control for high-order fully actuated nonlinear multi-agent systems. Nonlinear Dynamics, 2025, 113: 29233–29246.

[25] You L, Qin K, Yue J, et al. Neural network-based fully distributed dynamic event-triggered formation-containment control for nonlinear multi-agent systems. Neurocomputing, 2025, 642: 130324.

[26] Shi S, Wu S, Wei B. Neural-network-based event-triggered formation tracking for nonlinear multi-UAV systems with switching topologies under DoS attacks. IEEE Transactions on Automation Science and Engineering, 2025, 22: 11656-11667.

[27] Liu M, Zhang L, Zhao N, et al. Observer-based reachable set synthesis for multi-agent systems: A sampling-based distributed event-triggered strategy. Applied Mathematics and Computation, 2026, 510: 129683.

[28] Cai Y, Wang Y, Su H, et al. Bipartite leader-following consensus of linear multi-agent systems with unknown disturbances under directed graphs by double dynamic event-triggered mechanism. Applied Mathematics and Computation, 2025, 496: 129347.

[29] Li M, Long Y, Zhang K, et al. Time-varying dynamic event-triggered-based prescribed-time leader-following consensus for multi-agent systems with input saturation. Applied Mathematics and Computation, 2026, 508: 129630.

[30] Hou R, Jia L, Bu X, Peng C, Li J. Dynamic event-triggered formation-containment of heterogeneous multi-agent systems under DoS attacks via model-free adaptive control. Journal of the Franklin Institute, 2026, 363(6): 108516.

[31] Wang J, Hu Z, Zhang Y, Chen C L P, Liu Z, Chen K. Dual-channel adaptive event-triggered predefined-time consensus control for multi-agent systems. Nonlinear Dynamics, 2025, 113: 29681–29695.

[32] Xue S, Luo B, Liu D, et al. Neural network-based event-triggered integral reinforcement learning for constrained H_∞ tracking control with experience replay. Neurocomputing, 2022, 513: 25-35.

[33] Wang T, Zhang H, Sui S. Observer-based adaptive neural network event-triggered quantized control for active suspensions with actuator saturation. Neurocomputing, 2025, 614: 128770.

[34] Ding L, Han Q L, Ge X, Zhang X M. An overview of recent advances in event-triggered consensus of multiagent systems. IEEE Transactions on Cybernetics, 2018, 48(4): 1110-1123.

[35] Nowzari C, Garcia E, Cortés J. Event-triggered communication and control of networked systems for multi-agent consensus. Automatica, 2019, 105: 1-27.

[36] Chen J, Jiang P, Chen B, Zeng Z. Adaptive neural event-triggered consensus control for unknown nonlinear second-order delayed multi-agent systems. Neurocomputing, 2024, 598: 128067.

[37] Chen H, Xu Y, Fu M, Zhang G, Dong L, Min X. Distributed adaptive NN formation control for networked uncertain USVs with asynchronous edge-based dynamic event-triggered communication mechanism. Nonlinear Dynamics, 2026, 114: https://doi.org/10.1007/s11071-026-12239-8.

[38] Hou Z, Zhou Z, Zhang J, Wang W, Tang Y. Self-tuning dynamic event-triggered consensus control for multi-agent systems and its implementation via self-triggering. ISA Transactions, 2026, 173: 93–101.

[39] Zhang Y, Man J, Sheng Y, Lai J, Zeng Z. Dynamic edge-event-based consensus of nonlinear multi-agent systems with sampled-data measurement. ISA Transactions, 2026, in press. doi:10.1016/j.isatra.2026.10.005.